Luminescence dating, geochemistry, and analysis of Pleistocene sediments from Specimen Cave, Naracoorte, S.A.

Thesis submitted in accordance with the requirements of the University of Adelaide for an Honours Degree in Environmental Geoscience

Racheal Evelyn Mahlknecht
November 2018

THE UNIVERSITY
of ADELAIDE

LUMINESCENCE DATING, GEOCHEMISTRY, AND ANALYSIS OF PLEISTOCENE SEDIMENTS FROM SPECIMEN CAVE, NARACOORTE, S.A

LUMINESCENCE DATING OF SPECIMEN CAVE

ABSTRACT

A digitised map was produced for Specimen Cave and used to indicate sediment sampling locations. Luminescence dating of the sediments provided constraint on the encompassed megafaunal inclusions to between 119.27±13.50 ka and 165.50±21.19 ka. Single grained OSL method provided better results for the type of sediment accumulation than multi-grained analysis. The TT-OSL dating method provided better results for the age extent of sediment accumulation than single grained OSL analysis. The most reliable OSL technique for Middle Pleistocene material was TT-OSL, because SG-OSL had reached its limits of dating of the cave sediments due to grain saturation. Sediment morphology, through visual assessment and SEM images, displayed collisional wear patterns consistent with aeolian transport. Sediment input to the cave system was via pitfall entrances. Lithology was determined for 90 samples with characteristics used to compare provenance to known regional samples. Geochemical analysis of the cave sediments was used to assess; in situ sediment similarities horizontally between cave areas; provenance related to nearby caves; and provenance to local area deposits with only minor similarities detected. Organic residue was determined in the sediment samples but no pollen was present for palaeo-environment investigation. Deposition in the cave occurred during MIS 6 and MIS 5 in conditions of low ice volume, increased; CO^2, temperatures, and water table volumes, alongside decreased dust, sea level regression and continental uplift.

KEYWORDS

Luminescence, OSL, TT-OSL, geochemistry, Pleistocene sediments, Naracoorte, cave, palaeoenvironment, megafauna.

Word count excluding references, tables and captions: 7997

Table of Contents

LIST OF FIGURES AND TABLES

INTRODUCTION

Specimen Cave is a part of the Naracoorte Cave system in South Australia situated on private property. In 1908 megafaunal fossil deposits were uncovered, but aside from minor exploration, identification of a few discovered species, mapping (1959) and unpublished dating of cave flowstone, very little work has been completed at the cave (Reed and Bourne, 2000). Based on unpublished U-Th series dates of 136 ka and 139 ka (R. Weij, 2018, pers. comm., University of Melbourne, unpublished data, with permission) the cave fills a piece of the unrepresented, 100 ka to 200 ka, period in the Naracoorte Caves regional history for megafaunal successions and environmental conditions.

Numerical age dating of the accumulated cave sediments was used to constrain the age of the encompassed fossils and timing of local megafaunal extinction(s). The ages were also used to validate the temporal sequence of the cave in regional history and the suitability of selected luminescence techniques on materials from the Middle Pleistocene.

Samples collected from Specimen Cave were separated into fractions for use in two different luminescence dating techniques of single-grain optically stimulated luminescence (SG-OSL) and thermally transferred OSL (TT-OSL) and applied to quartz grains. Methodology of OSL procedures was evaluated through multigrain analysis, coupled with a comparison of SG-OSL, and contrasted with TT-OSL techniques for reliability and accuracy.

Sediment dynamics and infill sequence formation in the cave were established using grain size analysis, visual descriptions, morphology, and the construction of stratigraphic logs, to a depth of one metre, across four areas. Scanning electron micrographs were produced for surface assessment of individual grains to ascertain sediment transportation method(s).

Geochemical methods for palaeo-environment (provenance of sediments and palaeo-climate) of; X-ray diffraction (XRD), for mineralogy of the samples taken; X-ray Fluorescence (XRF) for chemical composition, both individual samples and ITRAX scanning of sediment core

lengths, were performed at an external facility. Palaeo-vegetation, through pollen analysis,

for past environmental conditions was performed. Geochemical analysis elucidates changes

in the local environment, habitat and climatic conditions surrounding the caves.

Cave mapping by hand, modified to a digitised output in metric, was undertaken and

combined with sediment data, for a comprehensive chronostratigraphic log and cave

representation. Collectively these analyses form a comprehensive site history including

changes in palaeo-environmental conditions and potential reasons for megafaunal extinction.

BACKGROUND

Geology

The Naracoorte Cave systems, in the southeast of South Australia, are 1.1 million years old,

set in the soft karst Gambier Limestone formation (Webb, Grimes, & Osborne, 2003; White

& Webb, 2015). The region was emptied of water, between 700-800 ka, due to continental

uplift of the southern margin of Australia, changing the region from a coastal environment to

an inland setting over that time frame (Lewis, 2017).

South Australia was subject to the Kanawinka Fault line that trends in a northwest–southeast

direction through the region traversing the Gambier Limestone formation (Fig 1), the fault

caused fracturing in the surrounding areas (Webb et al., 2003). These fractures allowed

groundwater and meteoric fluids to penetrate and create solutional flow waters of $CaCO_3$

(Dept. Environment & Heritage, 2001; Webb et al., 2003) The dissolution of the Gambier

Limestone generated the open cave spaces, and reformed as more compact (less porous)

speleothems and flowstone layers in the caves (DEH, 2001). Surface openings formed, wider

than the fault line cracks, permitting the influx of sediments from external sources, to begin

deposition in the newly formed cave spaces, accumulating the sediment record from the

surrounding areas (Webb et al., 2003). Many caves make up the Naracoorte caves area,

including Grant Hall, Victoria Fossil Chamber, and neighbouring Wet and Blanche Caves, which are local to the cave of interest, Specimen Cave, in either proximity and/or encompassing age (Forbes & Bestland, 2007).
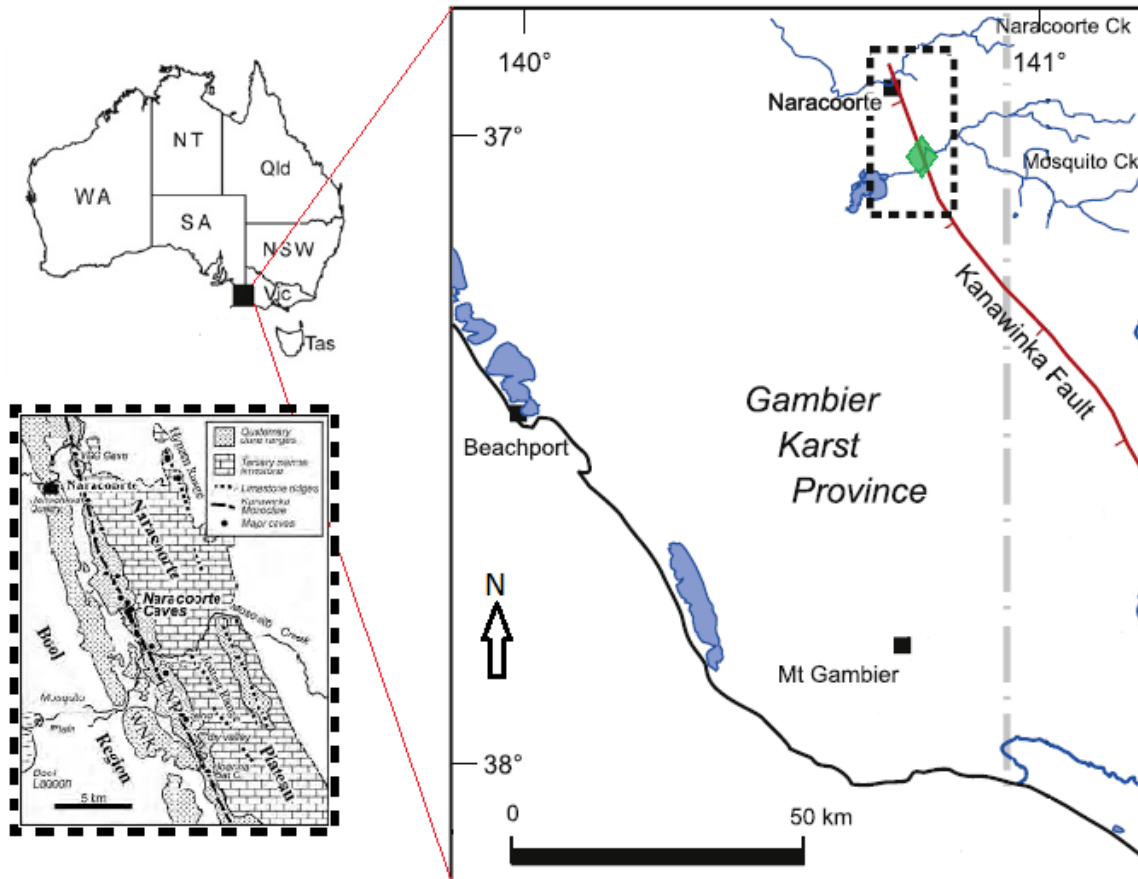
Figure 1. Naracoorte Caves area and surrounds, Lower Southeast, South Australia. The Kanawinka Fault traverses the region in a northwest-southeast direction (red line). Naracoorte Caves (green diamond) and the geology of local caves area (inset) (Adapted from Grimes & White, 2004; White & Webb, 2015).

Site

Specimen Cave (datum 5U35), located on private property, is a part of the Naracoorte Cave system, situated ~11km from the township of Naracoorte along the limestone coast (DEH, 2001). Very little site-specific work has been carried out at Specimen Cave since its original fossil discovery in 1908 (Reed & Bourne, 2000). A scanned copy of a map of Specimen Cave, draw by the Cave Exploration Group of South Australia (CEGSA) in 1959, was located (E. Reed, 2018, pers. comm.) (Fig. S1).

The surrounding Naracoorte Caves precinct has been variously dated and analysed over many decades. Fossil remains found in the caves, older than the limits of radiocarbon dating (~50,000 years) cannot be directly dated. With the cave setting considered to be around 136 ka (R. Weij, 2018 pers. comm.), modern methods were applied to the selected sediment sequences that encompass the fossils, for indirect dating. As more innovative dating methods are created and improved upon, more reliable numerical age constraints can be achieved. Dating of Specimen Cave was undertaken using state of the art luminescence techniques.

Luminescence

Luminescence dating techniques, OSL, based on Aitken (1998), and TT-OSL, from Wang Wintle, & Lu (2006), are used on quartz and feldspar grains. Upper boundaries to dating are based on an individual sand grains maximum saturation limit and range from ~150 ka for OSL to ~1 Ma for TT-OSL, further advances have improved accuracy of the techniques, reducing error margins (Chapot et al., 2017; Wallinga & Cunningham, 2015; Zander & Hilgers, 2013). Quartz grains from Australian sources need amended criteria applied for reliable dating outcomes. Study of Australian sediment conditions can provide information to assist in site specific grain dating, whereby criteria and procedural adjustments can be made for local preconditions.

Sediments

The cave system is made up of several caves of differing sizes, with varying sediment accumulation depths, which have been sampled for studies into sediment origin, and compared to both local and remote surface sources (Darrénougué et al., 2009; Forbes & Bestland, 2007; Macken et al., 2011). The caves area and sediment accretions have been linked to Murray River sediment input, with additions from regional red-brown earths (RBEs), and sands (Barrie, 1997; Forbes & Bestland, 2007). Wet Cave and Grant Hall, in

Victoria Fossil Cave, sit either side of the missing time scale, aged at <100 Ka and >200 ka respectively and can be used for sedimentary comparison. Entrance type affects sediment input to caves with the most common form in the area being vertical solution pipes and doline set pitfall openings (Webb et al., 2003). Provenance for the sediments in the surrounding caves display a mix of local and distant sources, but not all sediment origins have been completed and Specimen Cave sediments have not previously been analysed. Sediment provenance has been based on both visual descriptions and geochemical analysis.

Geochemistry

A few studies have incorporated geochemical methods for the areas both in, and around, the caves at Naracoorte, with Forbes & Bestland (2007) being one of the more notable. Geochemical assays of X-ray diffraction (XRD), for bulk sample mineral content, X-ray fluorescence (XRF) for bulk sample element composition, including rare earth elements (REEs), combined with palynology (pollen) and organic content, has been assessed in some caves and surface areas (Darrénougué et al., 2009; Forbes & Bestland, 2007). Surface XRF of core samples, using the Itrax scanner at ANSTO has not been carry out for Naracoorte Caves. Previous evidence can be employed to analyse the palaeoenvironment, palaeoclimate and sediment provenance for Specimen Cave, to provide a comprehensive representation of the sites past, and coupled with age dating, fitting the cave temporally into the Naracoorte Caves history.

METHODS

Investigation of Specimen Cave was undertaken using modern geoscientific methods to record and constrain ages of deposition, and in turn, the age of enclosed megafaunal fossils, which can be then related to their abundance and extinction event(s). A comprehensive site history, including cave mapping and digital reconstruction, luminescence age dating and

comparisons of applied methodologies, combined with sedimentology and geochemical methods, has been performed on/at the site for temporal, palaeo -environmental and -climatic conditions. Unless otherwise stated all analysis was performed at the University of Adelaide.

Site

The main cave was remapped, and set to Datum 5U35, by hand using a Lecia laser range finder centre line walk-and-measure method (SI), combined with outlining and adjustment of a scanned copy of the original map CEG 1119 (Fig S1) using CorelDRAW[©] 2018 (L. Reed pers. comm. 2018; Grimes, 1997; Wookey, Atkinson, and Day, 1995). In the lower section of the cave five samples (Spec18-1 to Spec18-5) were obtained from the sediment cone for dating and dosimetry, collection details in SI with spacing set out in Fig. S2. In situ gamma spectra recordings were taken for each sample site (Arnold, et. al, 2012).

Sediment sample collection consisted of 90 small samples of <30 g each for colour, sorting and grain feature analysis (Fig. S6a, b). Further sample collection for XRF, XRD, and grain size analysis, of 25 large samples (Z1 to Z25) from 80-160 g each, and 10 pot samples (P1 - P10) of >50 g each for palynology. Aluminium U-channel (1cm cross section) was cut to desired lengths by hacksaw, each length was pushed or hammered into position and a piece of wire was used to cut the samples from the sediment face. A total length of 1.09 m in three separate sections of U-channel was collected in Areas 1-2, with Section 1 overlapping Section 2 by ~17 cm, and Section 3 being stand-alone.

Photographic records, were taken throughout sample collection, including 364 specific photographs to produce a 3D composite image, and modified using editing software (SI).

Luminescence

All luminescence samples were prepared and analysed at Prescott Environmental Luminescence Laboratory (PELL), based on Aitken (1998) with modifications, under dark

(red) lighting conditions. All dose determination sets were performed on Risø TL/OSL-DA-20 Reader (Risø 2).

Preparation of five sediment samples (Spec18-1 to 5) was completed using methods detailed in Supplementary Information (SI). The 125-180 μm quartz fraction was utilised for equivalent dose estimation and dating experiments. Sediments surrounding the main sample were used for effective water content and dosimetry (SI) (Table S5).

Multi-grain (MG)-OSL loading of grains to flat, 3 mm oil masked aluminium discs, multiple grains per disc at 12 discs of sample Spec18-4, with 3 discs per temperature at 4 different temperatures (160, 180, 200, 220°C), general sensitivity determination performed using single-aliquot regenerative dose (SAR) protocol (Murray & Wintle, 2000). Samples were run with the green (532 nm) laser at 90% strength, with Hoya filter U340 x 7.5 mm, and the quartz window in. MG analysis was performed using Analyst v3.14$^{©}$ combined analysis program (Duller, 2015).

Single grain (SG), TT-OSL and dose recovery test (DRT) samples were loaded on aluminium discs and were run with the green (532 nm) laser at 90% strength, with Hoya filter U340 x 7.5 mm, and the quartz window out, following SAR protocols set out in Table 1 (Murray & Wintle, 2000; Wang, 2006). OSL DRT had extra steps for grain bleaching prior to the dosing cycle, of blue LED at 90% at 30°C for 1000 s, with two rounds with 6000 s pause in between. SG-OSL DRT at a given dose of 1140 s, with measurements made on four discs of Spec18-4, followed by a further two discs of the same sample at a later date. A total of 42 discs were analysed for SG-OSL covering all five Spec18 samples for equivalent dose (D_e) determinations. SG-TT-OSL DRT at a given dose of 900 s, with measurements made on 6 discs of Spec18-2. A total of 24 discs were run for TT-OSL covering three samples (Spec18-2, -3, -4) for D_e determinations.

Table 1. SAR protocols for single-grain OSL and TT-OSL signal determination and dose recovery tests for age calculations. Ln and Lx represent the natural and regenerative-dose signal measurements, respectively. Tn and Tx refer correspondingly to the test dose signals measured after the original L$_n$ and L$_x$ signals. OSL DRT extra steps for grain bleaching prior to dosing cycle, blue LED at 90% at 30°C for 1000 s, two rounds with 6000 s pause in between (based on, Aitken, 1998; Murray & Wintle, 2000; Wang, et al., 2006).

Step	Single Grain-OSL	OSL	Step	Single-Grain-TT-OSL	TT-OSL
DRT [a]	Given dose (beta 1140 s)		DRT [a]	Given dose (beta 900 s)	
1	Preheat to 260°C 10 s		1	Preheat to 260°C 10 s	
2	Stimulate with green laser at 125°C for 2 s (90% power)	L$_n$ or L$_x$	2	Stimulate with green laser at 125°C for 3 s (90% power)	
3	Give a test dose (beta 98 s)		3	Preheat to 260°C 10s	
4	Preheat to 200°C 10 s		4	Stimulate with green laser at 125°C for 3 s (90% power)	L$_n$ or L$_x$
5	Stimulate with green laser at 125°C for 2 s (90% power) - OSL		5	Stimulate with blue LEDs at 280°C for 400 s (90% power)	
6	Give a test dose (adjust beta input signal times for curve formation)		6	Give a test dose (adjust beta input signal times for curve formation)	
7	Preheat to 260°C 10 s		7	Preheat to 260°C 10 s	
8	Stimulate with green laser at 125°C for 2 s (90% power) - OSL	T$_n$ or T$_x$	8	Stimulate with green laser at 125°C for 3s (90% power)	
9	Repeat 3-8 for dose response curve		9	Preheat to 260°C 10 s	
10	Repeat from 1 for new sample or DRT for dose recovery test		10	Stimulate with green laser at 125°C for 3 s (90% power)	T$_n$ or T$_x$
			11	Stimulate with blue LEDs at 280°C for 400 s (90% power)	
			12	Repeat 6-11 for dose response curve	
			13	Repeat from 1 for new sample or DRT for dose recovery test	

[a] Dose recovery test

Individual grain analysis was performed using Analyst v3.14© (Duller, 2015) and SAR Rejection Criteria spreadsheets (SI). After the equivalent dose (D_e) was spatially adjusted construction of radial plots, performed on Radial Plots v1.3© was completed. The computations for ages were performed using Hiro Average 2017, for CAM calculations, and R^{2}© for MAM calculations (MAM calculations completed by L. Arnold, pers. comm. 2018).

Sediments

Individual sediment samples were described and logged to form the stratigraphic lithology of the cave deposition to a depth of 1 m and 0.95 m in Areas 1-2 and Areas 3-4 respectively (SI;

Table S6a, b). Grain size analysis was completed on 12 samples (Table 2) using stacking sieves for collection of fractions of <500, <250, <125, <63, <38, >38 μm (SI). Photo-overlay of the sediment units was completed with CorelDRAW© 2018, using photographs from the aforementioned site records. Smear slides for petrography were prepared by placing a small sediment sample in ethanol on a slide, placing a cover slip on top and attaching with clear silicone to seal (adapted from: Kelts, 1998).

Quartz and cave samples were prepared (SI) for use in the XL30 Scanning Electron Microscope (SEM) at Adelaide Microscopy. Micrographs of quartz grains and cave sediment were produced for assessment of external morphology with Secondary Electron and contrast with backscattered electron (SI).

Geochemistry

Twelve of the large samples (Table 2) collected were processed (SI) and sent for XRF and XRD analysis at University of Wollongong, NSW. The 3 U-channel sections (SI) were sent for surface XRF (Itrax) scanning at ANSTO, Lucas Heights, NSW and further analysed (SI). Palynology (pollen) analysis of 4 samples was completed following a shortened pollen extraction method from Nguyen, et. al. (c2013) (SI) and examined under 400x and 600x microscope.

Table 2. Large Z sample selection for grain size analysis and XRF/XRD analysis.

Analysis	Sample Number											
GSA	Z25	Z23	Z21	Z19	Z17	Z15	Z13	Z11	Z9	Z6	Z3	Z1
XRF/XRD	Z24	Z22	Z20	Z18	Z16	Z14	Z12	Z11	Z8	Z6	Z4	Z1

RESULTS AND OBSERVATIONS

Investigation of Specimen Cave was undertaken using both qualitative and quantitative methods. Qualitatively, the stratigraphy of the cave sediment was logged in the excavated section and a new digitised map was produced. Quantitatively, numerical dating has been used to constrain the timing of sediment deposition. Combining the dating results and further geochemical assessments of the sediments, using X-ray Fluorescence (XRF), X-ray diffraction (XRD), organic content and pollen analysis, was completed to form a comprehensive chronostratigraphic record.

Site

The construction of the cave plan, cross section and selected lower cave sections of Specimen Cave (Fig. 2) was adapted from the original map (Fig. S1) and combined with new digital measurements. Site layout and interior features were adjusted and the depth aligned to the cave datum, 5U35. Spacing of the dating samples (Fig. S2); the distances in between each OSL sample and the surrounding cave, including roof heights and air spaces, for dose rate calculations, was mapped out for the lower cave section, between s and u (Fig. 2) of Specimen Cave.
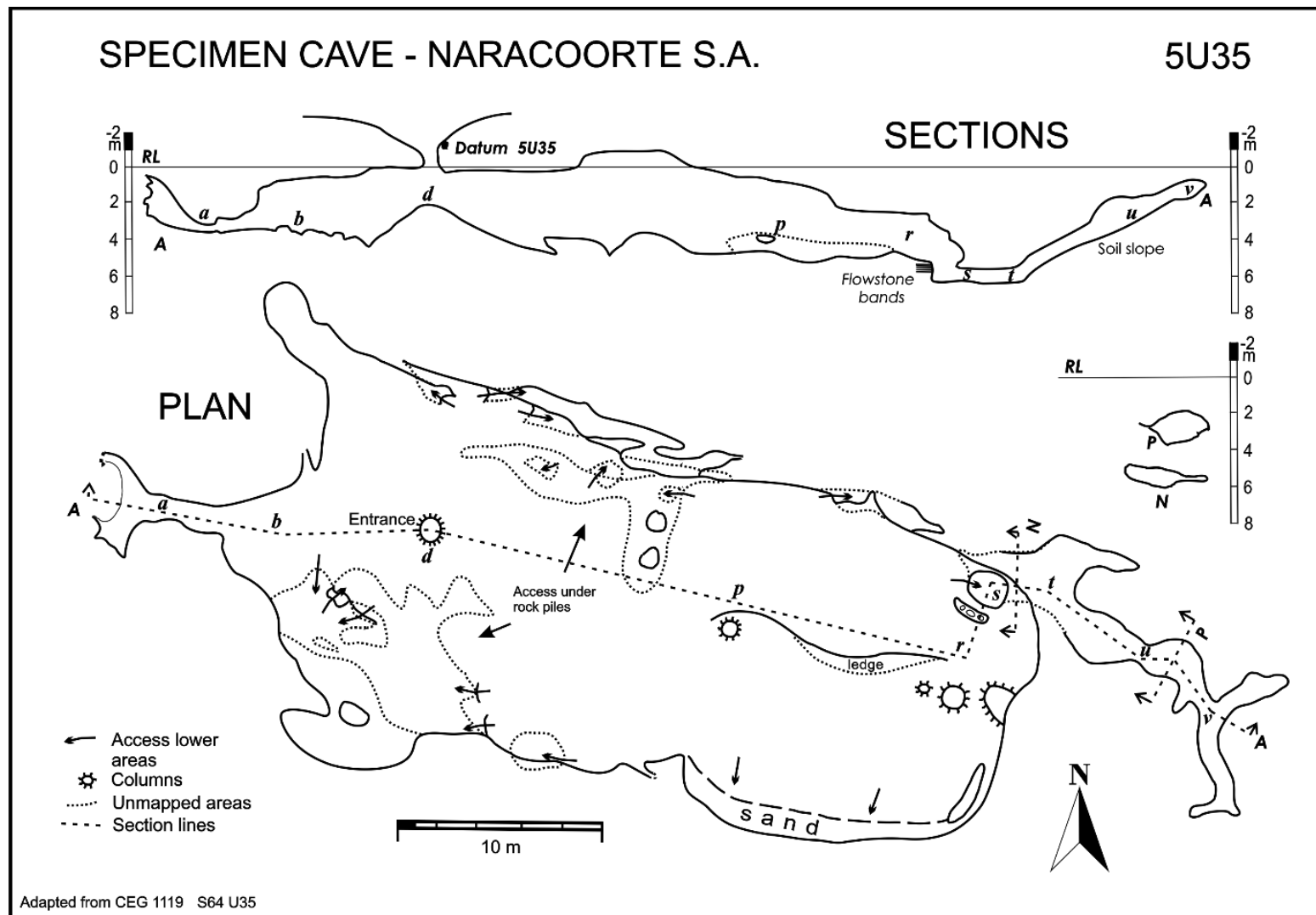
Figure 2. Plan and cross sections of Specimen Cave, Naracoorte, South Australia, datum 5U35. Excavation of Areas 1-2 on south west face between *t* and *u* located in lower passage and of Areas 3-4 at drop down between *r* and s incorporating flowstone bands. In cave datum located on rim of dropdown (above *s*) (adapted from scanned copy of CEG SA 1119 map, 1959 and combined with updated measurements 2018).

Luminescence

Multi-grain (MG)-OSL performed on 12 discs of sample Spec18-4 returned a temperature

sensitivity at 200°C that was applied to further SG-OSL analysis (Fig. 3).

Dose recovery tests (DRT) were performed on Spec18-4 for OSL, in two runs, on 400 and

200 grain sets, and Spec18-2 for TT-OSL, of one run of 600 grains, with 100 grains lost due

to a disc positioning error (Fig S3). DRT determined the sensitivity and suitability of the set

single-aliquot regenerative dose (SAR) protocol parameters applied (Murray & Wintle, 2000)

and confirmation of the selected temperature for further SG measurements on quartz grains

from the site. A total of 42 discs were run for SG-OSL across the five Spec18 samples, and a

further 24 discs for TT-OSL across 3 samples (Spec18-2, Spec18-3, Spec18-4).

Analysis for OSL, of 800 grains per run, except Spec18-5 with 1000 grains, had a grain

acceptance rate of 6-11% across the five samples. A higher grain rejection rate occurred with

the TT-OSL, with an acceptance rate of only 3-6%. Reasonably high numbers of saturated

grains were rejected during analysis on all Spec18 samples, with Spec18-4 being the highest

at 4%. Slow grains were also a major factor in rejection in the analysis with an overall loss

between 5-12%, especially for TT-OSL signals. Some super grains, with extended trapping

capacity, had very large (irradiation) signals recovered and were found distributed throughout

the samples. Summaries of SAR rejection criteria for all DRTs are in Tables S1 and S2, and

for standard OSL and TT-OSL analysis, in Tables S3 and S4 respectively.

Original radial plots, based on the Central Age Model (CAM), displayed high overdispersion

(OD), and as using the CAM overestimates the underlying ages, the Minimum Age Model

(MAM) was instead applied (Wallinga & Cunningham, 2015). Modelling of ages used MAM

3 (except Spec18-2 used MAM-4) for all age determinations. Although Spec18-1 and

Spec18-4 were not supported on MAM-3 over CAM, the MAM dates were used because of

the high OD of results. MAM calculations were based on a 20% OD rate (Wallinga &

Cunningham, 2015), based on the average of ideal well bleached samples from nearby

Blanche and Alexandra caves. Radial plots, indicating minimum D_e values with 2 sigma (σ)

error bands, were produced, for DRT (Fig. S3), and all OSL and TT-OSL Spec18 samples

based on MAM (Fig. 4). Dosimetry measurements for the cave sediments and surrounds,

recorded in Table S5, were used for sediment age calculations.
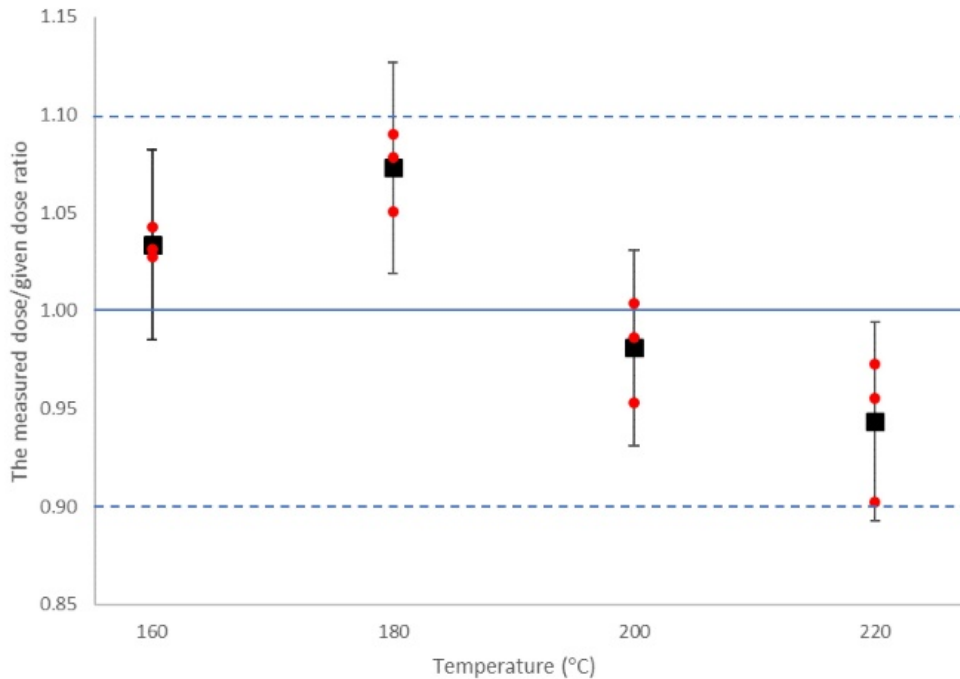
Figure 3. Results of multi-grain preheat dose recovery test for 212-250 μm quartz sample Spec18-4. Aliquots were measured in sets of three, using four different preheat temperatures ranging from 160C to 220C held for 10s (red dots). Black squares indicate the measured dose/given dose ratios calculated for each set of aliquots with 2 sigma error bars. The range of acceptability is between 0.9 and 1.1 (dashed lines), with unity of 1 as the target value (solid line). These results were checked for sensitivity changes.

Ages determined were between the youngest of 119.27±13.50 ka (second shallowest) to the

oldest at 165.50±21.19 ka (deepest) (Table 3). Dates determined were compared, both in age

and cave profile depth, to unpublished dates of 139.02 ± 6.79 ka and 136.23 ± 15.66 ka (R.

Weij, pers. comm. 2018), obtained from U-series dating of the flowstone that sits over the

sediments of interest (Fig. 5). Dates from each level are, mostly, within tolerances of each

other in the 1σ standard error range.
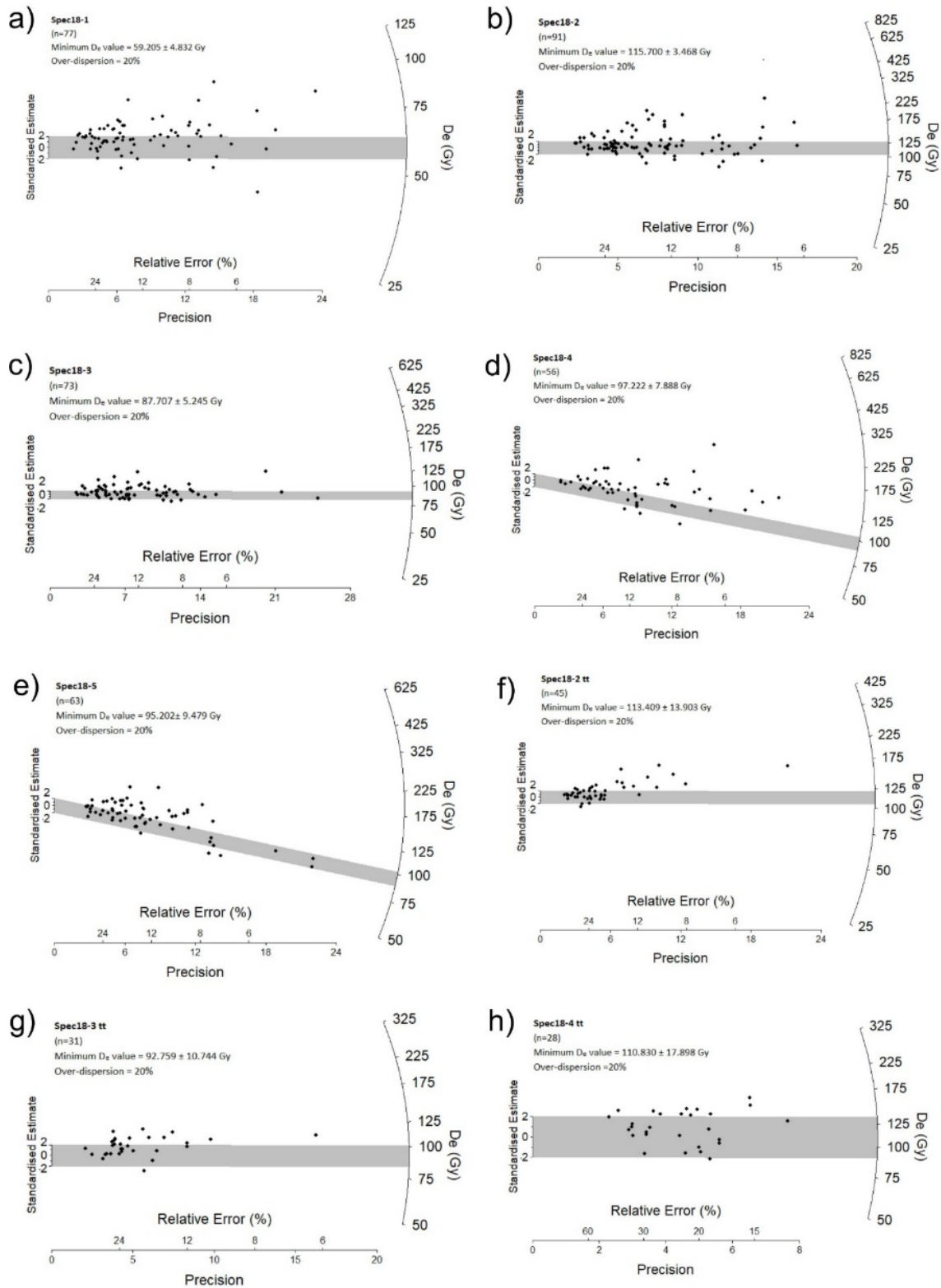
Figure 4. Specimen Cave radial plots a) to e) OSL, f) to h) TT-OSL. Radial plots based on MAM-3 (except b MAM-4).

Table 3. Luminescence dating results using MAM 3 with a 20% overdispersion for each sample, in profile depth order.

Spec18-	OSL		TT-OSL		Cave
	Age (ka)	se ± (ka) [a]	Age (ka)	se ± (ka) [a]	Depth (m)
1	124.15	12.37	-	-	7.31
5	119.27	13.50	-	-	7.45
4	124.51	12.06	141.93	24.12	7.70
2	150.82 [b]	9.33	147.83	19.81	7.79
3	156.49	12.67	165.50	21.19	8.05

[a] Standard error at 1σ

[b] MAM 4
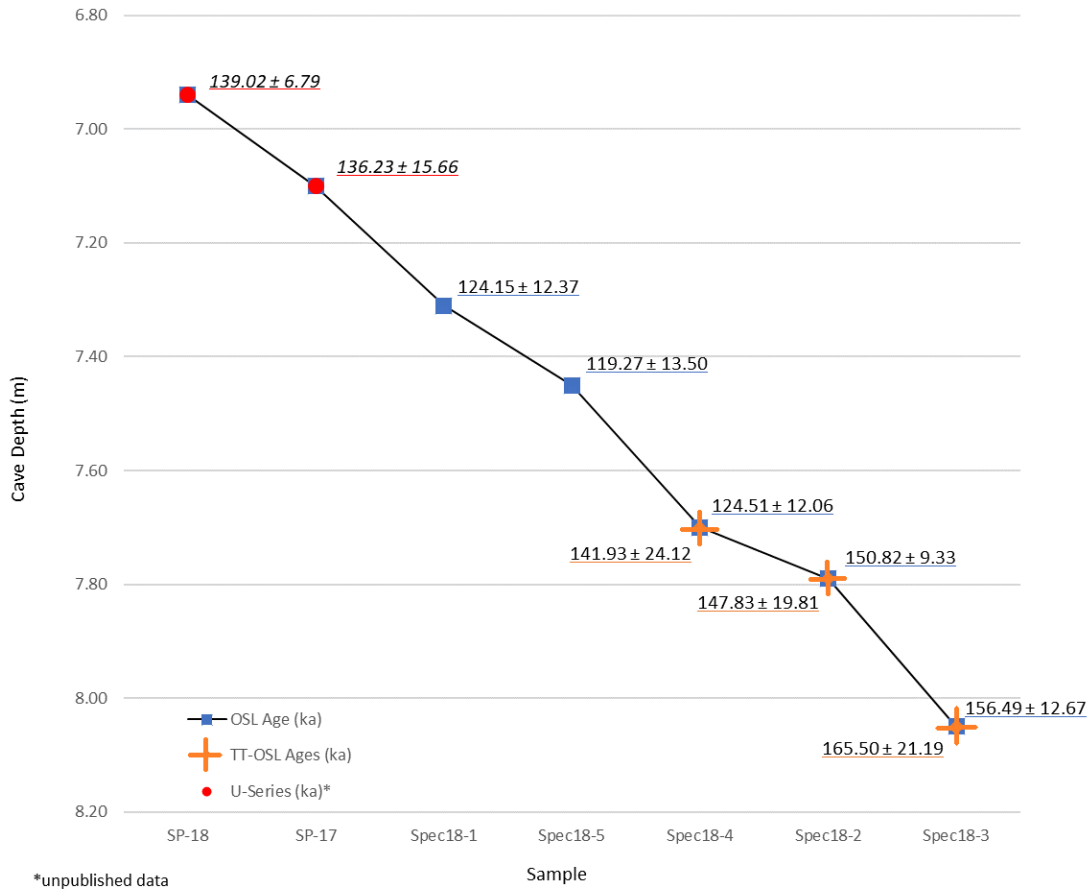
Figure 5. OSL (blue square) and TT-OSL (orange cross) age comparison depths in cave sediments related to U-series ages on flowstone (red circle) (Unpublished data: R. Weij, pers. comm. 2018, University of Melbourne, with permission).

Sedimentology

Distinct banding in the sediments and some flowstone layers were used to arbitrarily denote units (Fig. 6). These units were further subdivided and sampled in an order from top to bottom of each profile space, and logged as collected with a description (Tables S6a, b). Some distinct sand lenses with very fine sands were noted in the profile of Area 1-2. Flowstone layers end either abruptly, as they reach the cave wall, or peter out within the five-metre gap between Area 3-4 and Area 1-2. Unit 6, flowstone at 751 cm cave depth, is the only complete flowstone that crosses the whole five-metre wide range, ending in Area 1. Age samples Spec18-1 and Spec18-5 are above Unit 6 and the rest of the samples are below. In general, the sediments were fine grain clays to coarse grains of quartz, well sorted, mature in texture, and composition with colours in the 5YR range mostly 4/6 or 5/6 in hue/chroma. Area 1-2 is predominantly unconsolidated yellowish-red with upper red-brown and odd reddish-yellow sediment bands. Area 3-4 has a mainly reddish-yellow upper section, interspersed with consolidated green-grey to dark brown flowstone layers, whereas the lower section is yellowish-red deposits with a broad segment of closely spaced flowstone-sediment layering (Fig. 7). Full descriptions, based on Boggs (2009, 2014), of each layer are in supplementary information Tables S6a and S6b. Great size variation within, and between, the areas was not evident, but most of the sediment layers had flaky pieces of cave limestone and fossil fragments intermingled.

Grain Size Analysis

Grain Size Analysis (GSA) (Table S7) performed on the Z-samples listed in Table 1, displays a courser grain size of > 0.50 mm for up to 38% of the total sediment measured for each sample, with the exception of Z17. Sample Z17 had > 0.50 mm grain size for 52% as it contained greater amounts of cave limestone and fossilised bone fragments (Fig. 8; Fig. S4).
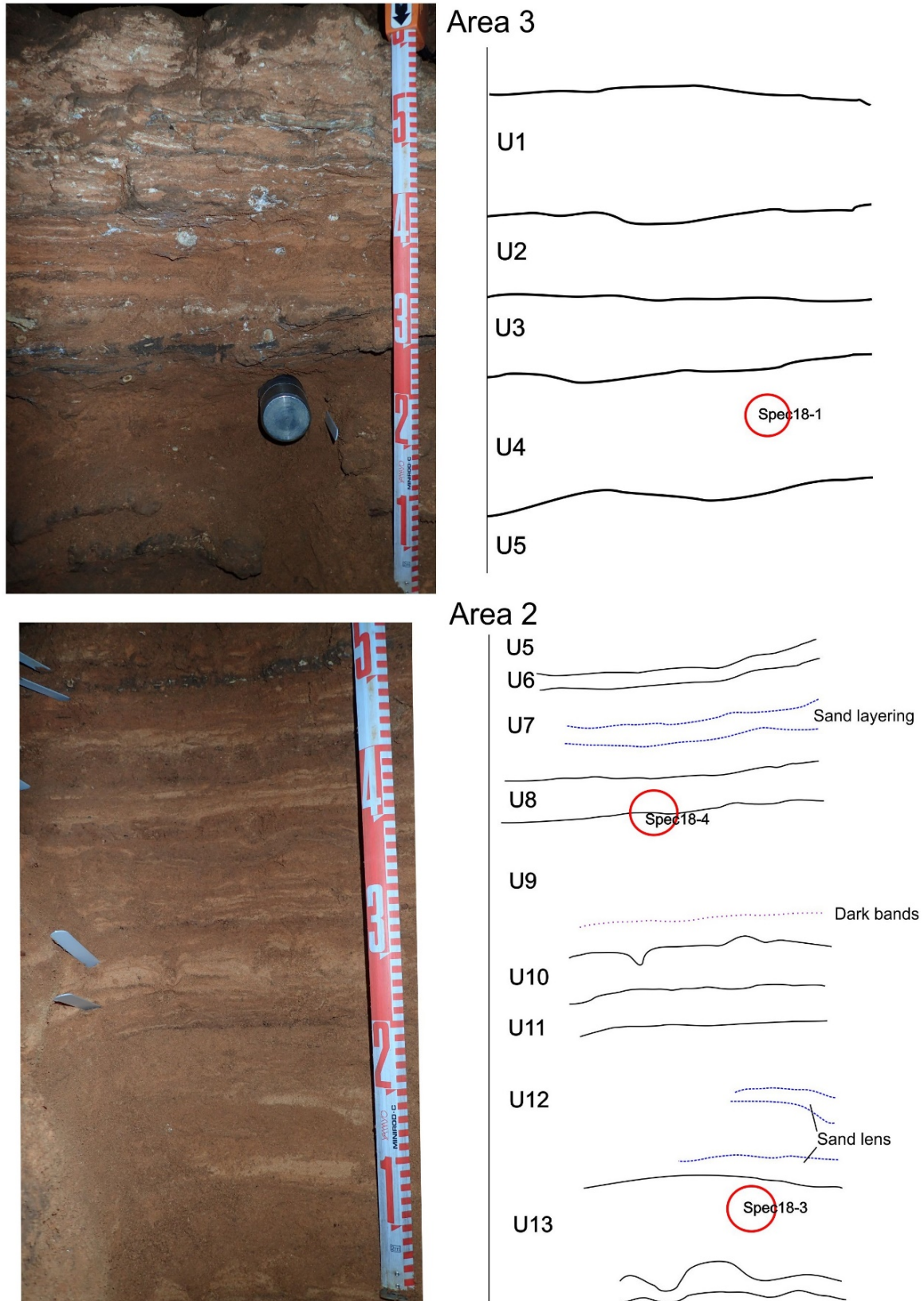
Figure 6. Unit overlay of the sediment cone of Area 2 (bottom) and Area 3 (top). Total depth of 1.23 m across the combined sections, with a cave depth of 6.86 m to 8.09 m. Individual units arbitrarily assigned based on an in situ, visual assessment. Spec18 sample locations indicated (red circles). Unit 6 is the only complete speleothem across the whole five-metre-wide area.
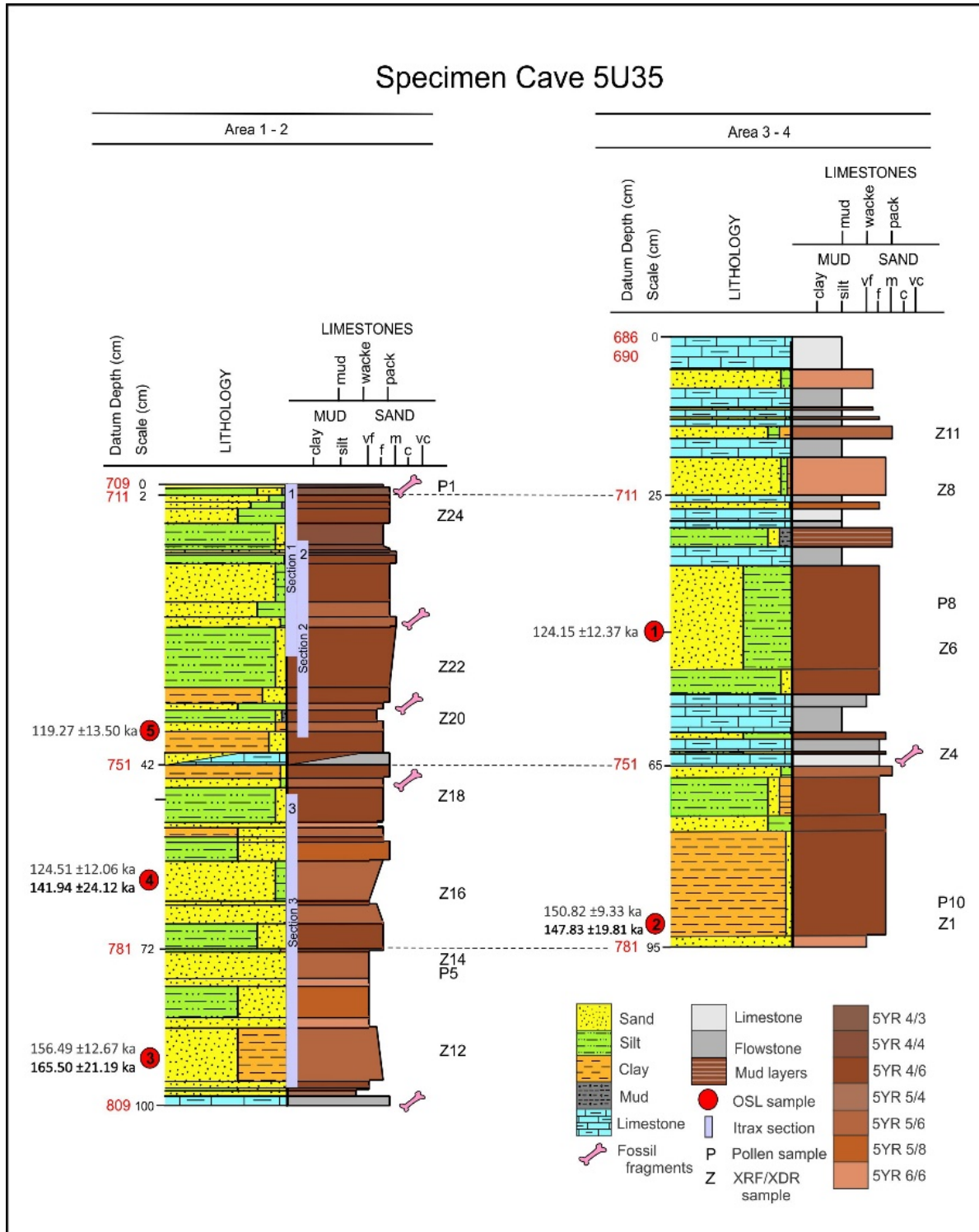
Figure 7. Chronostratigraphic log: Contacts between unconsolidated sediments are only sharp where contact is next to a flowstone layer. Almost all flowstone deposits had distinct banded layering and were generally horizontal in nature. Unit 6 (limestone at 751 cm cave depth) is the only complete speleothem that crosses the whole (five-metre-wide) area.

Skewness (asymmetry) of the samples was negative, exhibited as a tail pull to the finer sizes, and a peak curve centred on 0.25 mm grain size. Kurtosis (peakedness) of the average of all the samples sized, sat between slightly peaked to normal (leptokurtic to mesokurtic). The two most extreme samples Z6, with a positive kurtosis (leptokurtic), and Z21, with a negative kurtosis (platykurtic) (Fig. 9) are presented for the full sediment range.
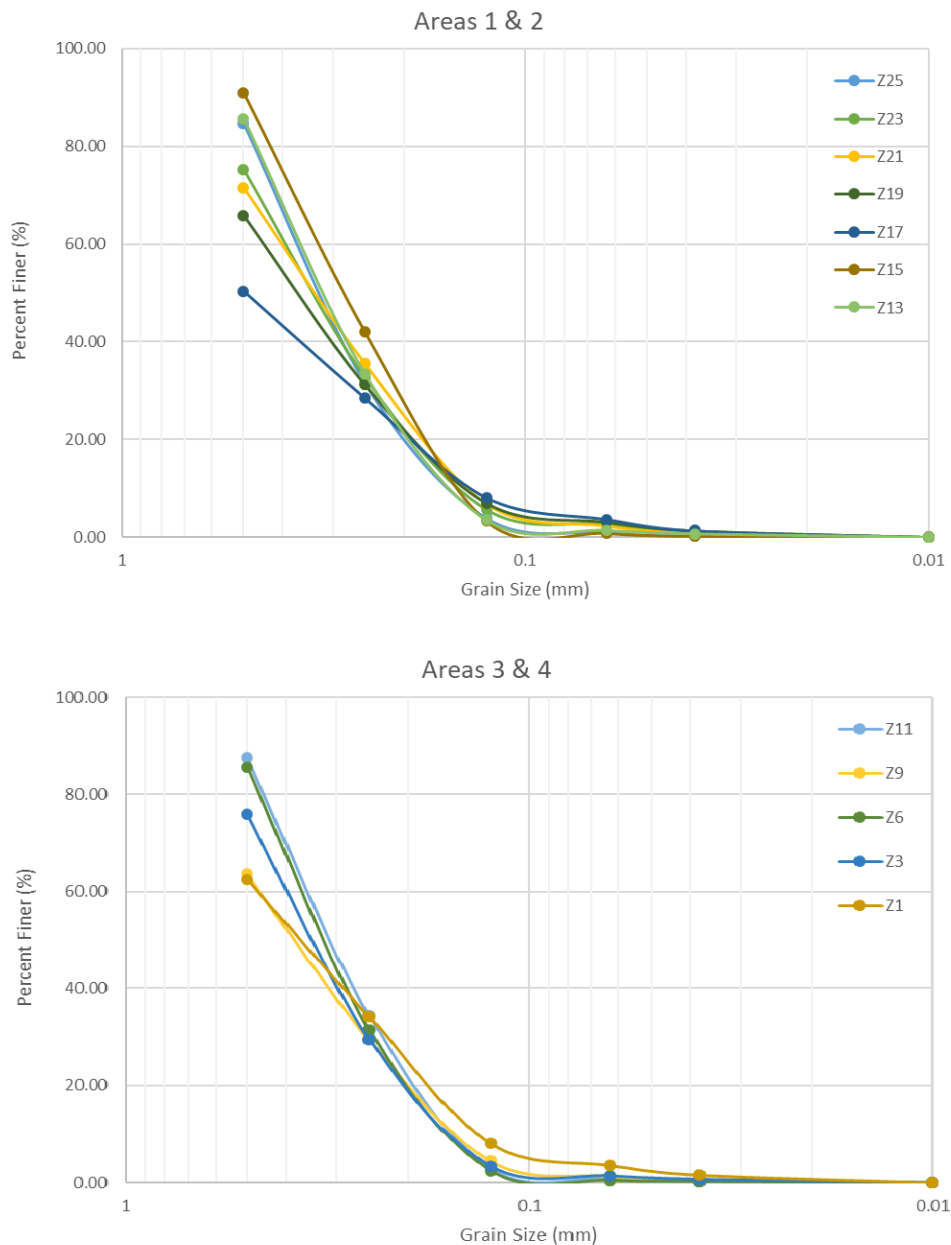
Figure 8. Specimen Cave sediment grain (particle) size analysis of percent finer and log scale size. Sediments from adjacent sets, Area 1 – 2 (top), display consistent grain size composition in each layer at depths ranging from 7.13 m (Z25) to 7.90 m (Z13). Sample Z17 contained greater amounts of cave limestone and fossilised bone fragments. Area 3 – 4 (bottom) display consistent grain size composition in each layer at depths ranging from 7.03 m (Z11) to 7.78 m (Z1).
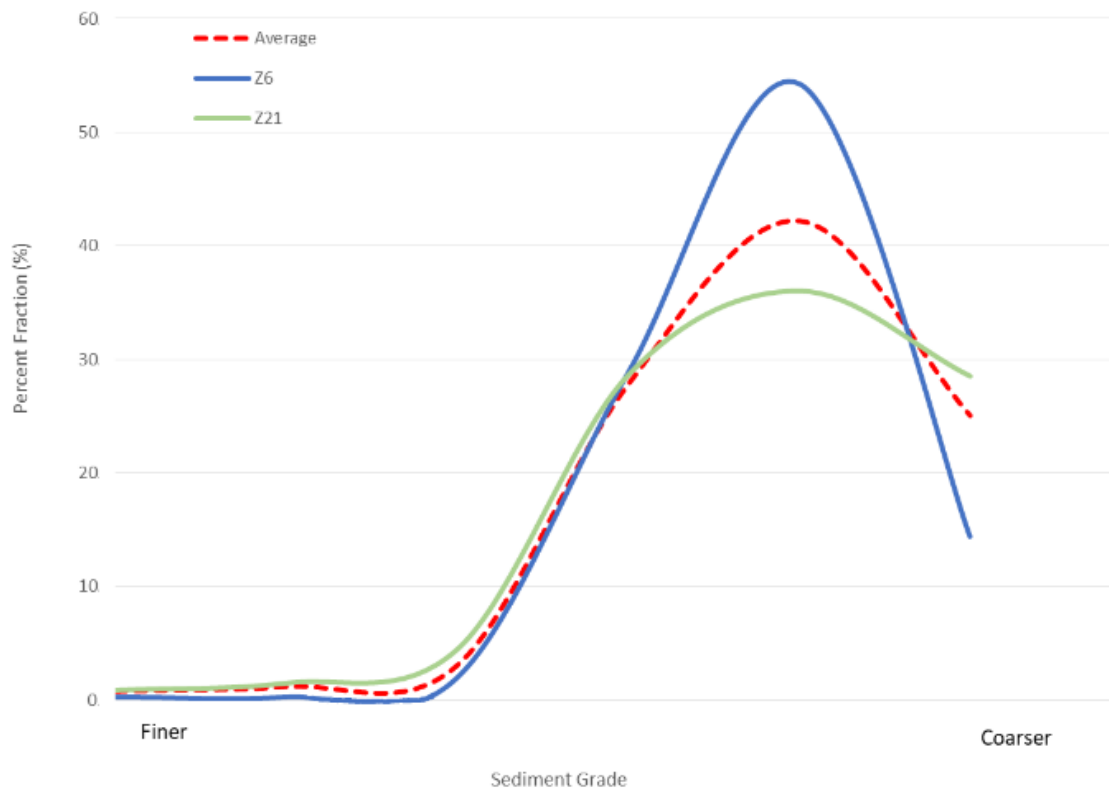
Figure 9. Skewness (measure of symmetry); high, low and average samples for Specimen Cave, the peak aligns with 0.25 mm grain size. All samples negatively skewed towards a courser grain size value. Kurtosis (peakedness); Samples Z6, positive kurtosis (leptokurtic); Z21 negative kurtosis (platykurtic); Average of all sediment samples assessed sat between slightly peaked to normal kurtosis (leptokurtic to mesokurtic).

SEM Cave sediments

Grain surface texture can aid in determining the mode of transport a grain has been relocated by, Cave samples were compared to SEM images appearing in literature, for example, Darrénougué et al. (2009) and Vos, Vandenberghe, & Elsen (2014). The SEM images of the cave sediments (Fig. 10) display a mixture of grain surface textures from spherical (equant), with v-shaped pock marks, through sub-rounded to sub-angular, elongate grains, with conchoidal fractures.
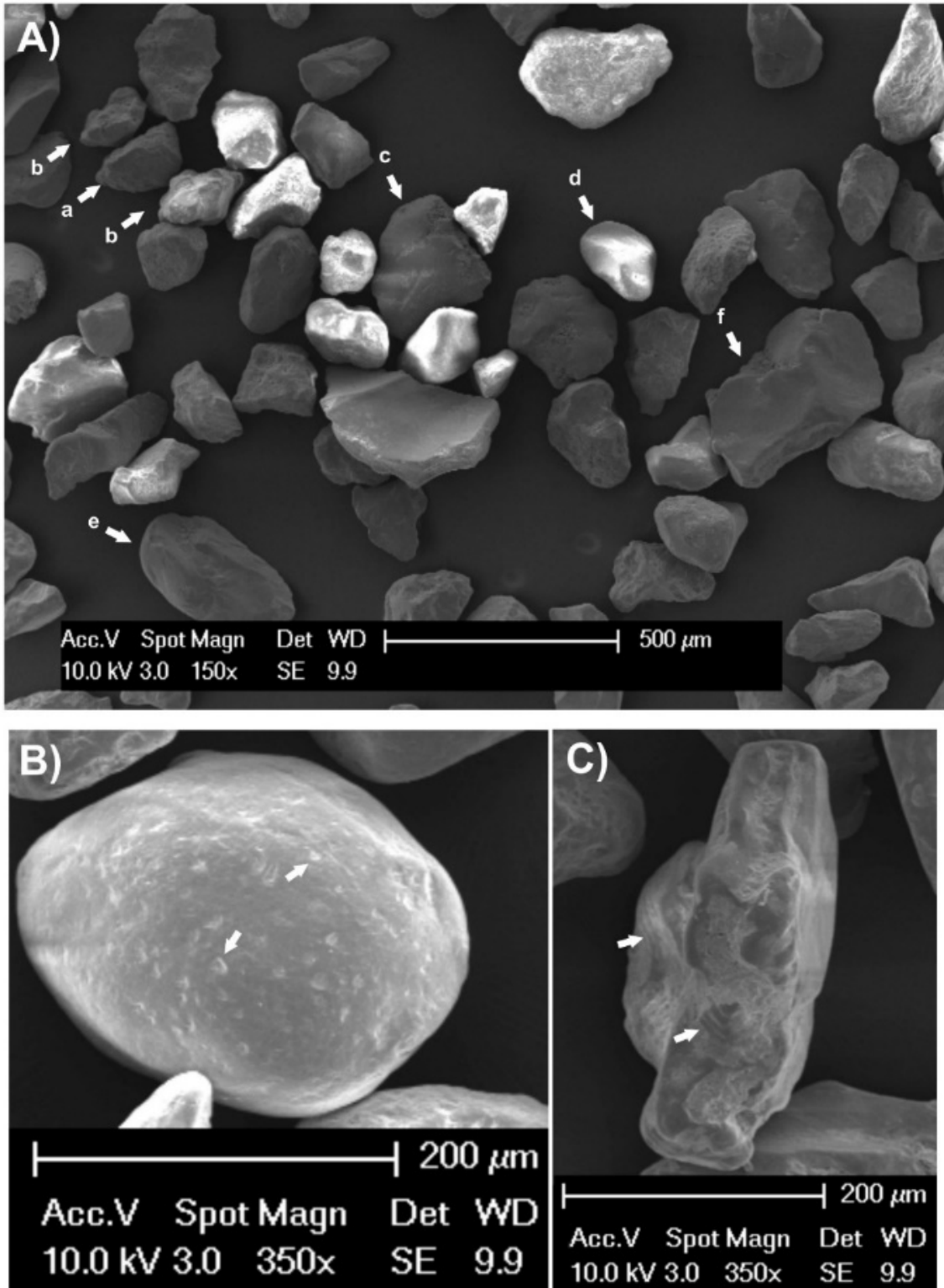
Figure 10. Scanning Electron Micrographs of quartz grains. (A) Spec18-1 - SE010, 212-250 μm; multiple grains, a) angular, b) sub-angular, c) sub-angular-sub-rounded, d) rounded, e) elongate, f) sub-angular - sub-rounded oblate (B) Spec18-3 - SE005, 90-212 μm; collisional v-shaped pock marks rounded grain (C) Spec18-4 - SE020, 212-250 μm: conchoidal fractures sub-angular/sub-rounded grain.

Geochemistry

Elemental, mineral and organic assessment on the cave sediments were evaluated by XRD, XRF, Itrax, and palynology methods. Comparison of the large Z samples, to assess similarity, were done for; Z8 to Z24; Z6 to Z22; and Z1 to Z14, as they correlate across both areas for being roughly at the same depth in the sediment profile. Matching Z samples to the Itrax core depths and Spec18 sample placement, provided; Z20 for Spec18-5; Z16 for Spec18-4; and Z12 for Spec18-3. Equivalent Z samples to Spec18 sample depths gave; Z1 for Spec18-2 (corresponding to Z14 in Area 1-2) and Z6 for Spec18-1 (corresponding to Z22 in Area 1-2).

XRD

Mineralogy of the sediments were predominantly quartz (77-90%) with microcline (3-10%) and calcite (1-7%) appearing in all samples (Fig. 11). Common minerals across the samples were chlorite, illite and albite appearing in at least eight samples. Minor amounts of orthoclase (Z4 and Z12) and hematite (four samples, with three of those from Area 1-2) were detected. Labradorite was in three samples, two from Area 1-2 (Z18, Z20) and one in Area 3-4 (Z1). Kaolinite appears in sample Z22 Area 1-2, which tracks correspondingly to Z6 in Area 3-4 where the mineral is not present.

XRF

XRF analysis of samples provided information on organic content, through loss on ignition (LOI) analysis, and similarities or differences between the equivalent depth Z samples from the two areas. LOI is a method used to determine the percentage of organic content in the sample (Donaldson, 2016). LOI from the cave sediments was between 2.7 to 7.2% per sample (Table 4). Samples Z1 compared to Z14 displayed very similar elemental and oxide levels spanning across the laminae, whereas Z8 to Z24, Z6 to Z22 do not provide as many similarities between them (Table 5).
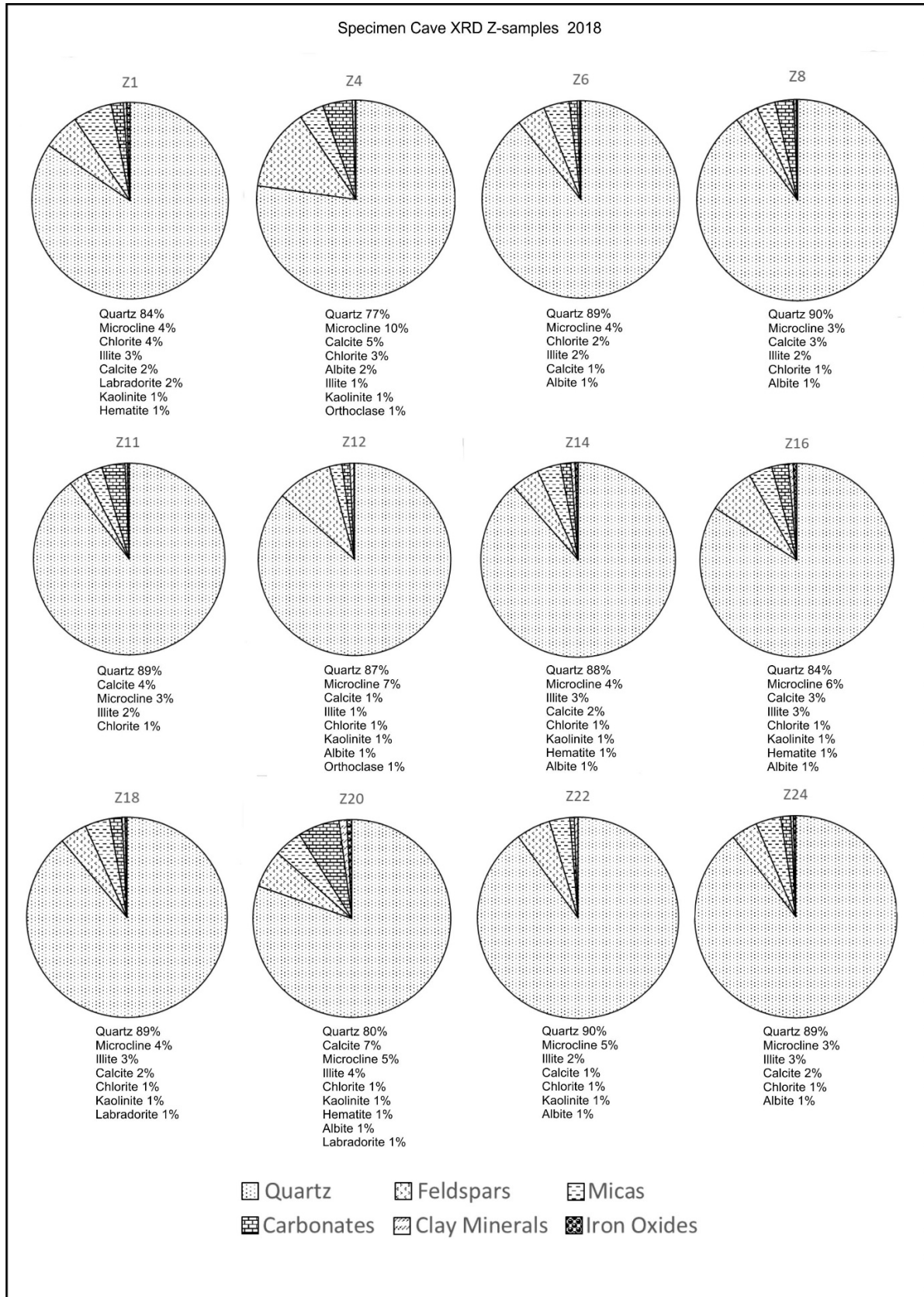
Figure 11. X-ray diffraction (XRD) pie charts of cave sediment percent mineral content and key mineral groups. Areas 3-4, samples Z11 (top) -Z1 (bottom) and Areas 1-2. samples Z24 (top) -Z12 (bottom).

Table 4. X-ray fluorescence (XRF) table of oxides Areas 3-4, samples Z11 (top) -Z1 (bottom) and Areas 1-2. samples Z24 (top) -Z12 (bottom).

Field number Spec18	Na2O %	MgO %	Al2O3 %	SiO2 %	P2O5 %	SO3 %	K2O %	CaO %	TiO2 %	MnO %	Fe2O3 %	LOI %
Z1	0.10	0.06	5.96	81.95	0.46	0.01	0.39	2.30	0.36	0.02	3.36	5.46
Z4	0.25	0.04	3.94	82.02	0.69	0.04	0.23	4.25	0.26	0.01	2.84	5.53
Z6	0.13	0.00	1.90	90.03	0.97	0.02	0.19	2.37	0.16	0.02	2.19	2.80
Z8	0.00	0.00	1.46	90.70	0.18	0.01	0.15	2.80	0.13	0.01	2.10	2.93
Z11	0.00	0.00	1.37	88.29	0.14	0.02	0.15	3.54	0.11	0.01	2.21	3.54
Z12	0.08	0.00	2.78	89.18	0.19	0.01	0.21	1.60	0.20	0.01	2.41	2.74
Z14	0.34	0.06	4.32	83.94	1.07	0.02	0.35	2.90	0.29	0.02	2.65	4.19
Z16	0.08	0.07	5.69	79.60	0.12	0.03	0.35	2.21	0.33	0.02	3.24	5.22
Z18	0.12	0.04	4.10	84.33	0.40	0.01	0.28	2.43	0.26	0.01	2.75	4.29
Z20	0.54	0.12	5.24	76.08	1.48	0.03	0.34	6.21	0.31	0.02	2.93	7.21
Z22	0.17	0.01	3.89	86.54	0.65	0.02	0.24	1.66	0.27	0.01	2.67	3.31
Z24	0.43	0.04	2.48	84.37	1.98	0.03	0.24	4.31	0.22	0.02	2.06	3.53

Table 5. X-ray fluorescence (XRF) table of elements. Areas 3-4, samples Z11 (top) -Z1 (bottom) and Areas 1-2. samples Z24 (top) -Z12 (bottom).

Field number Spec18	Cl ppm	V ppm	Cu ppm	Zn ppm	As ppm	Rb ppm	Sr ppm	Y ppm	Zr ppm	Ba ppm
Z1	222.8	59.4	8.8	21.8	14.6	25.7	23.7	20.0	173.0	162.4
Z4	140.6	42.7	9.3	23.8	11.4	15.7	20.8	13.7	166.9	105.4
Z6	167.3	16.4	12.0	28.4	5.1	9.7	20.2	6.7	100.6	110.6
Z8	77.5	17.7	11.1	10.9	3.7	7.3	13.2	4.5	79.5	47.6
Z11	86.8	13.0	15.0	9.3	3.2	7.1	14.6	4.0	52.6	97.8
Z12	87.5	26.3	8.8	11.2	6.9	12.0	14.6	10.3	129.5	84.6
Z14	138.6	40.0	9.6	31.6	9.2	20.0	28.9	15.2	146.5	156.6
Z16	117.9	58.8	7.4	15.7	14.0	23.8	22.6	18.4	154.7	138.1
Z18	117.3	42.8	11.3	18.9	10.0	17.5	20.8	13.8	133.2	138.7
Z20	289.0	52.6	8.0	37.1	12.3	21.7	38.5	17.5	156.1	200.7
Z22	206.4	39.6	7.9	24.3	9.4	15.4	19.9	13.4	190.0	138.6
Z24	406.4	26.1	12.5	41.6	4.6	12.9	39.5	8.9	171.0	139.9

ITRAX Analysis

All Itrax analysis was performed at a step speed of 10 s per 1 mm with no dwell time. Several indicators and proxies from the raw data have been separately evaluated.

A proxy for organic content is the molybdenum incoherent/coherent ratio (Mo (Inc/coh) or Mo-ratio) in which samples low in organic matter tend to contain heavier elements and cause more Mo coherent scattering, while lighter elements indicate high organic content resulting in more incoherent Mo scattering (Donaldson, 2016). Section 1 Itrax results shows distinct troughs that coincide with peaks of strontium (Sr) and calcium (Ca) and lows of silicon (Si) (Fig. 12). Similar patterns are observed in Sections 2 and 3 (Fig. 13; Fig. 14) although not as pronounced. Three Spec18 samples correlate to the Itrax core; Z12 to Spec18-3; Z16 to Spec18-4; and Z20 to Spec18-5.

Variations in the potassium/titanium (K/Ti) levels reveal changes in sediment provenance, largely controlled by sea-level changes, and climate, where higher ratios occur during interglacial periods (Wei, Liu, Li, Shao, & Liang, 2003). Results from K/Ti exhibit a variable depth ratio, with a distinct s-curve down Section 1 and 2, except in Section 3, which is variable but linear (Fig. S5). Comparison of the Si/Ti ratio, a measure of biogenic silica (aeolian input), where an increase to the right means increased sediment input from aeolian sources, and an increase left means a decrease in aeolian input (Croudace, Rindby, & Rothwell, 2006; Croudace & Rothwell, 2015). Itrax data from Section 1 and 2 mostly gave minor Si/Ti ratio variations in input (Fig. S6), with a major peak on Sec. 2 at 74 mm (itrax depth). Section 3 had three separate peaks (234 mm, 364 mm, and 479 mm), and one major trough (204 mm) which correlate with peaks and troughs of silicon, respectively.

Palynology

Palynology assay, useful for determination of past vegetation and climate, was negative for pollen in the four samples tested (Fig. 6; Table S8).
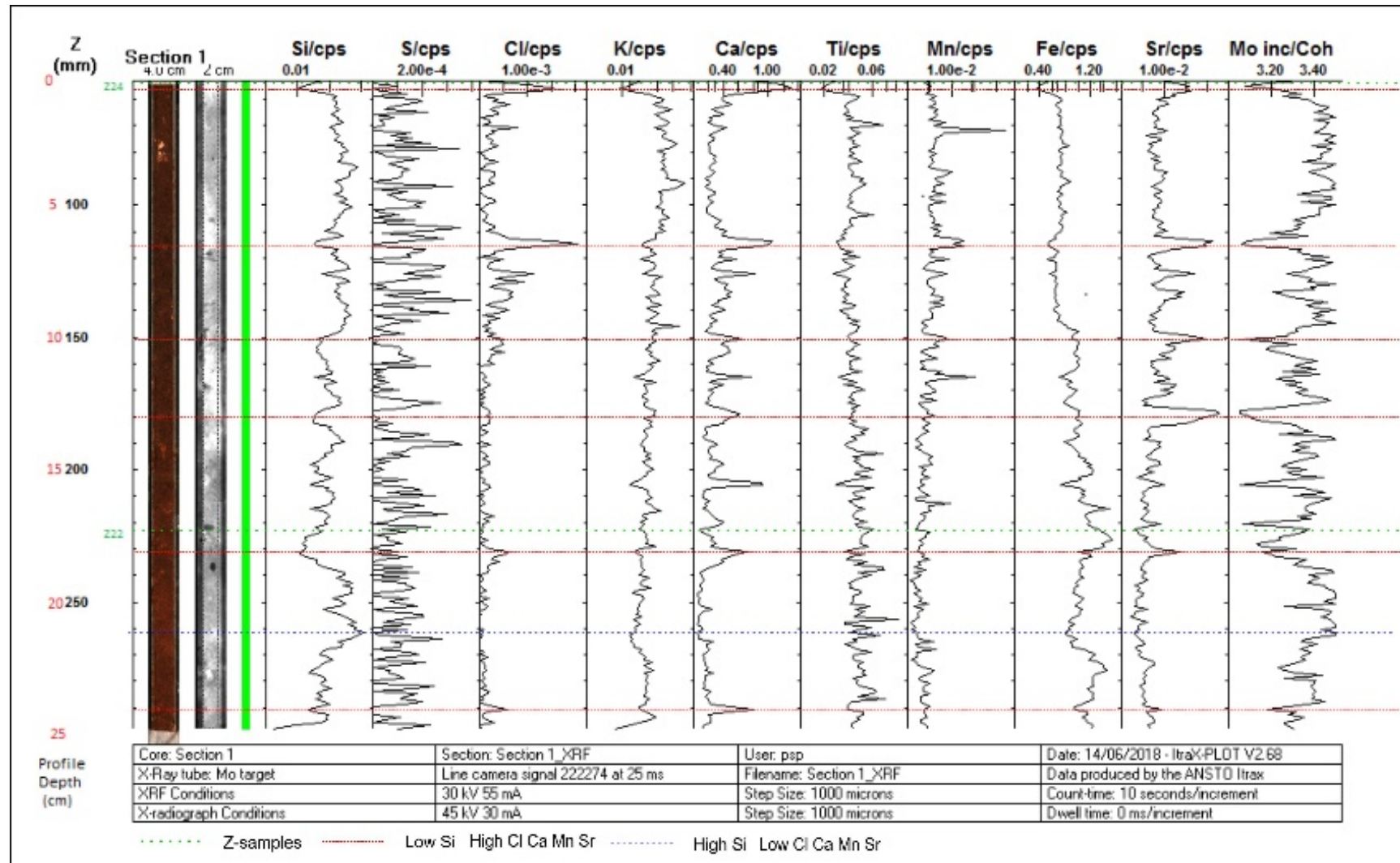
Figure 12. Itrax analysis section 1 - Optical image, X-radiograph, selected ITRAX-XRF results, and Mo Inc/Coh (as a measure of organic matter content) Z-samples (green dash) equivalent depth for separate XRF bulk analysis, correlation low Si to high K, Ti, Mn, Fe, Sr (red line); high Si to low Cl, K, Ca, Mn, Fe, Sr (blue dots) step speed, 10s per 1 mm, no dwell time (ANSTO, 2018).
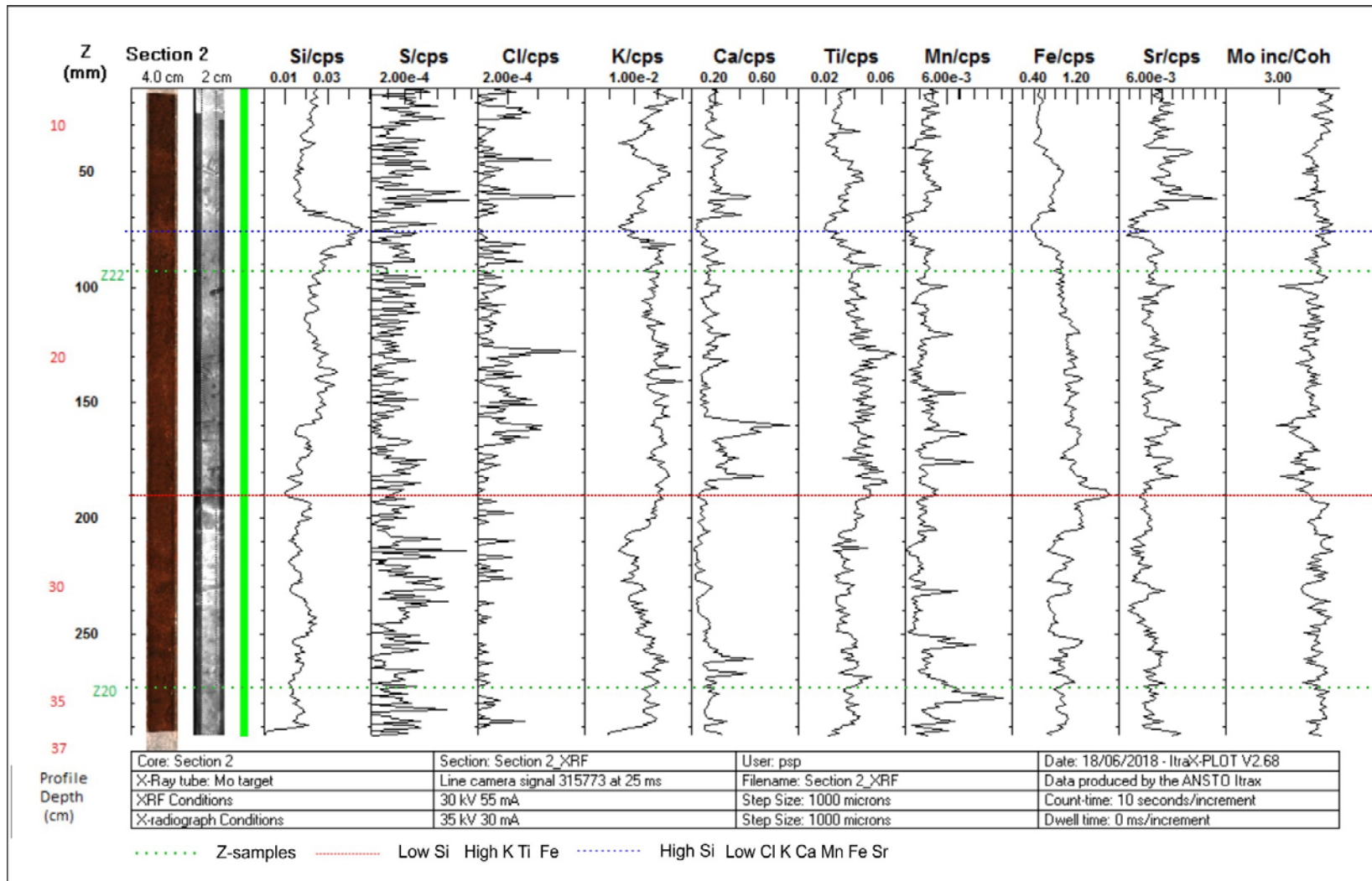
Figure 13. Itrax analysis section 2 - Optical image, X-radiograph, selected ITRAX-XRF results, and Mo Inc/Coh (as a measure of organic matter content) Z-samples (green dash) equivalent depth for separate XRF bulk analysis, correlation low Si to high K, Ti, Mn, Fe, Sr (red line); high Si to low Cl, K, Ca, Mn, Fe, Sr (blue dots) step speed, 10s per 1 mm, no dwell time (ANSTO, 2018).
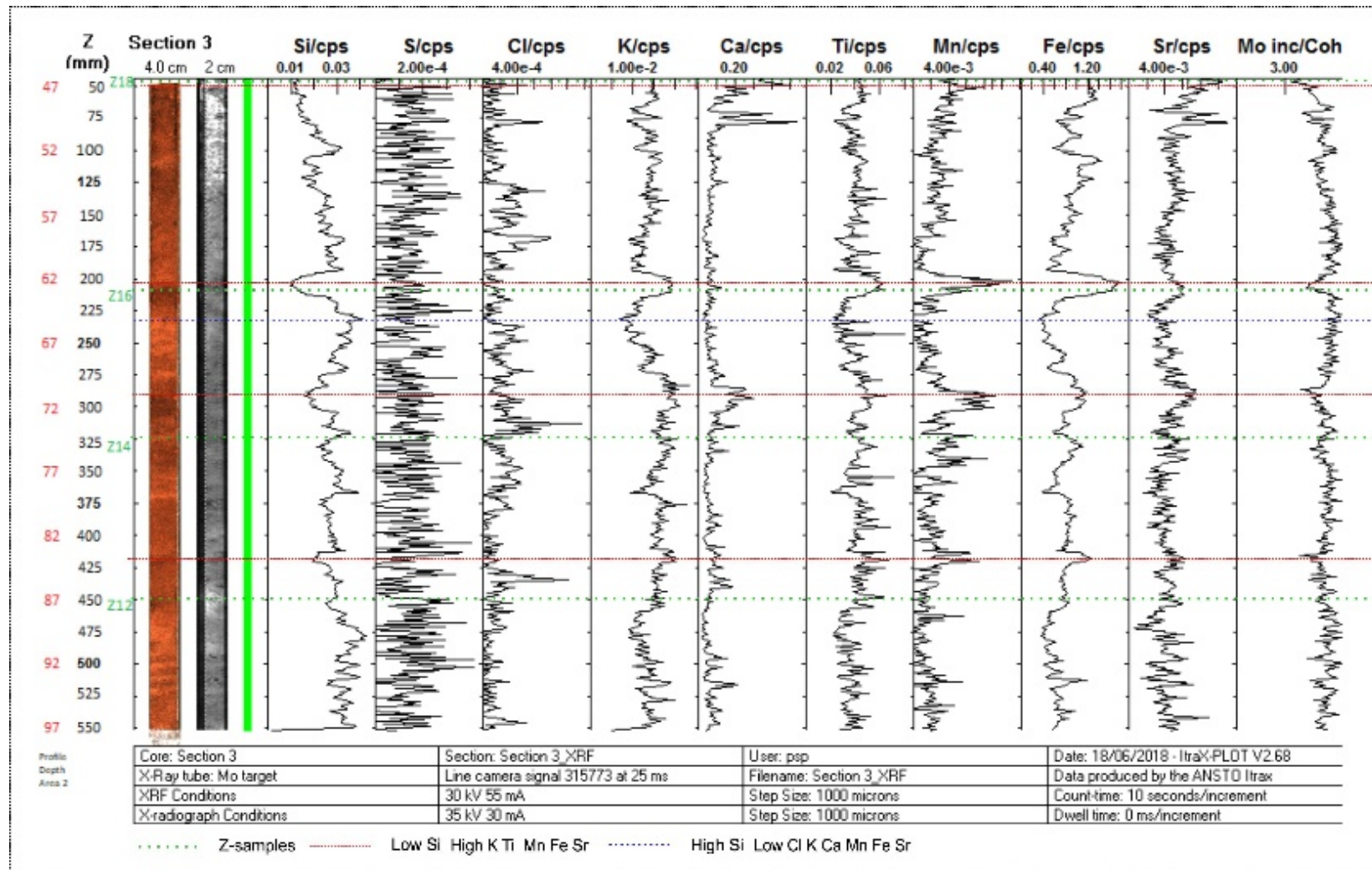
Figure 14. Itrax analysis section 3 - Optical image, X-radiograph, selected ITRAX-XRF results, and Mo Inc/Coh (as a measure of organic matter content). Z-samples (green dash) equivalent depth for separate XRF bulk analysis, correlation low Si to high K, Ti, Mn, Fe, Sr (red line); high Si to low Cl, K, Ca, Mn, Fe, Sr (blue dots) step speed, 10s per 1 mm, no dwell time (ANSTO, 2018).

Global Conditions: 210 ka to Present

Global conditions for the relevant time periods covering the age of Specimen Cave sediment ages, with error margins, indicate deposition during marine isotope stage (MIS) 6c/d through to MIS 5d/e (Fig. 15) (Railsback, Gibbard, Head, Voarintsoa, & Toucanne, 2015). MIS boundaries between cycles are; 7/6 at 191 ka; and 6/5 at 130 ka (Fig. 15) (Lisiecki & Raymo, 2005; Railsback et al., 2015). The evaluated sediments sit between primary dates of ~119 ka to ~166 ka, with an extended age error range of ~107 ka to ~187 ka, occurring during the Middle (126 - 781 ka) to Upper (11 - 126 ka) Pleistocene. These dates encompass the penultimate glacial period, from 185,000 to 130,000 years ago, followed by the last interglacial, concluding ~117,000 years ago, when the last glacial period (Weichsel) began (Rohling, et al., 2007; Railsback et al., 2015). The foremost change occurred around MIS5, 132,000 –117,000 years ago, which included MIS 5e (Eemian) with its peak at 123,000 years ago (Railsback et al., 2015). Unit 6 is constrained by the numerical ages of ~119 ka to ~142 ka ago, during this timeframe global mean surface temperatures climbed 1-2°C, carbon dioxide (CO_2) atmospheric levels were ~280 parts per million, dust concentrations were low, ice volumes were decreased, and as a result mean sea level were 4–6 m (with fluctuations up to 10 m) higher than at present (Fig. 16) (Rohling, et al., 2007; Dahl-Jensen, et al., 2013).
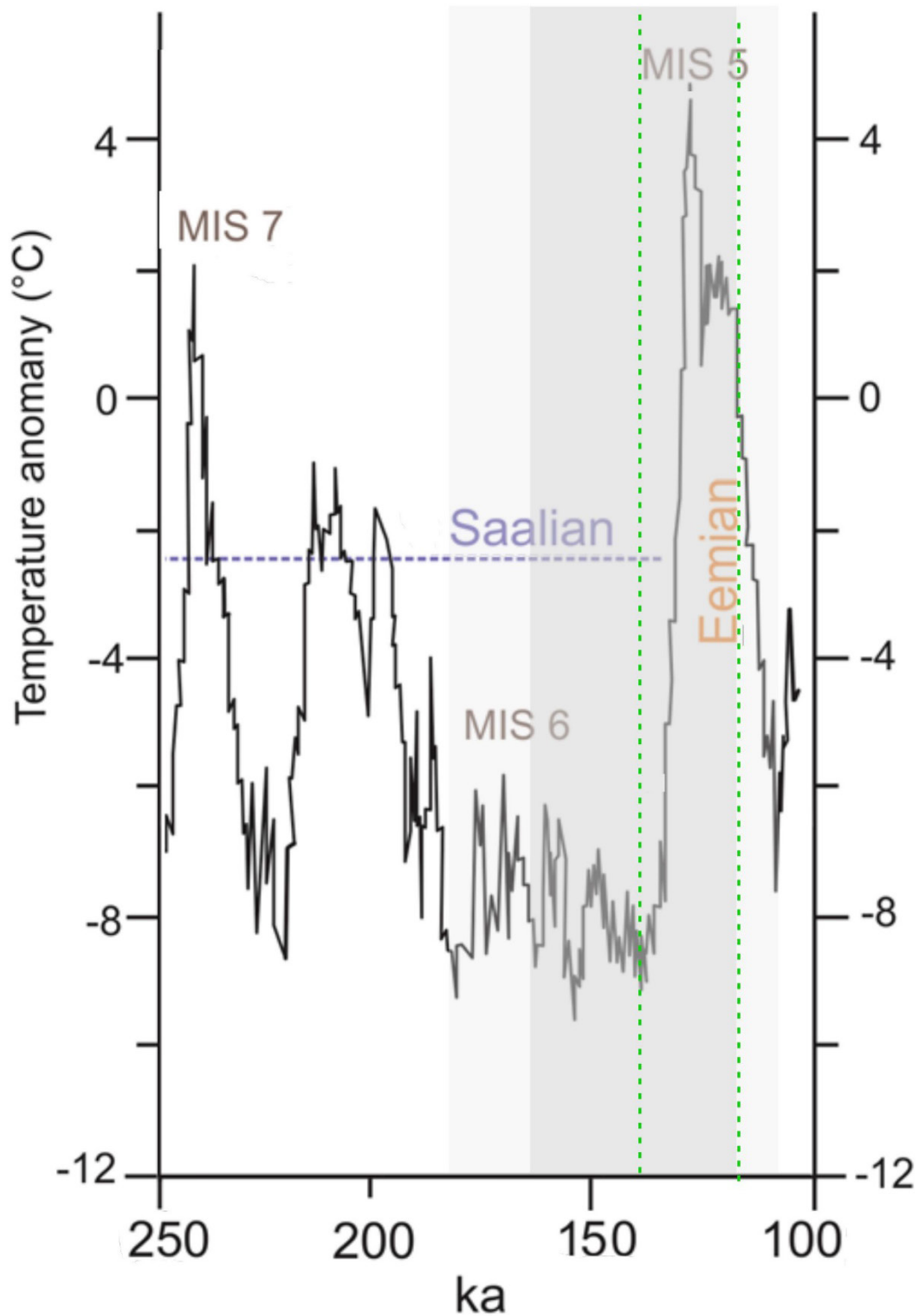
Figure 15. Marine isotope stages (MIS) for the period 100-250 ka ago. MIS boundaries between cycles 7/6 at 191 ka; and 6/5 at 130 ka. Specimen Cave sediment high/low ages (dark grey band) and error margins (light grey band) determined in this study, ages constraining Unit 6 from the stratigraphic log (green dashed lines) (adapted from Lauer & Weiss, 2018).
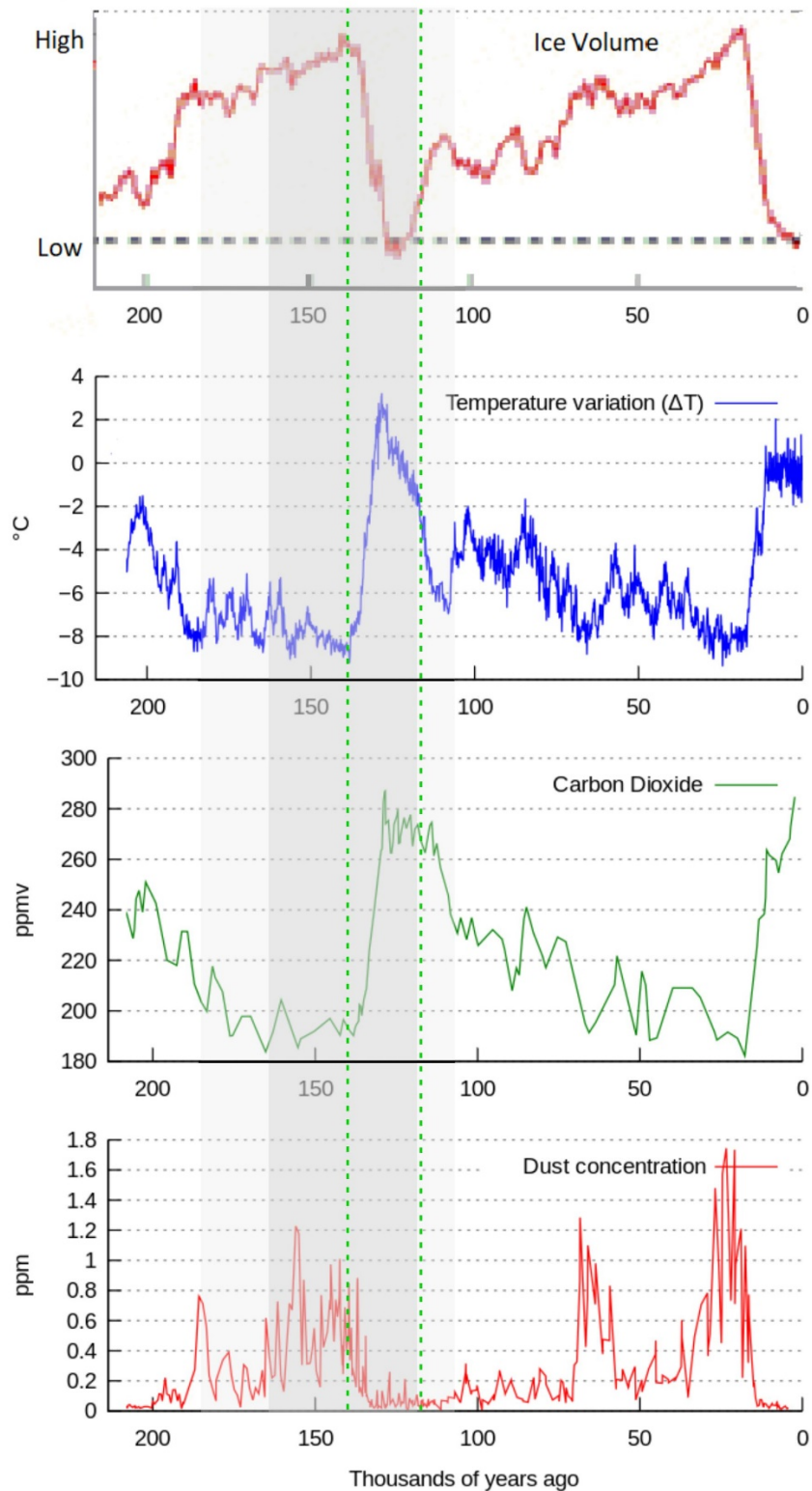
Figure 16. Ice volume, Temperature variation, carbon dioxide levels, and dust concentration for the period 0-210 ka. Specimen Cave sediment high/low ages (dark grey band) and error margins (light grey band) determined in this study, ages constraining Unit 6 from the stratigraphic log (green dashed lines) (adapted from Petit et al., 1999; Rohde c2008).

DISCUSSION

Site

The general cave map of Specimen Cave, remeasured and digitised, only covered some cross-sectional segments and will need to be completed for the remaining cave sections (Fig. 2 compared to Fig. S1). Luminescence dating of the site confirms the cave fills a piece of the missing temporal sequence of data from Quaternary studies done in the Naracoorte area.

Luminescence

Luminescence numerical dating of the quartz sediments provided constraint on the encompassed megafaunal inclusions to between 119.27 ± 13.50 ka to 156.49 ± 12.67 ka for SG-OSL, and to between 141.93 ± 24.12 ka and 165.50 ± 21.19 ka for TT-OSL (Table 3; Fig. 5). The age of the sediments in Specimen Cave were slightly lower than expected for the upper two samples but within tolerance of each other and the U-Th - series dates (139.02 ± 6.79 ka & 136.23 ± 15.66 ka) (Fig 5). The lowest three samples in the stratigraphy were closer to the expected age for their depth, and again, well within tolerances of each other. Spec18-4 dates of 124.51 ± 12.06 ka using SG-OSL, corresponded with 141.93 ± 24.12 ka using TT-OSL, these two dates are not as close together in age as achieved on samples Spec18-2 and Spec18-3 using the same two methods. The difference between the two Spec18-4 dates can be attributed to a high rejection rate of saturated grains, at 4%, removing the larger (older) D_e values (Table S3; Table S4). Spec18-4 TT-OSL provided a more reliable result as it is closer to the sample below (Spec18-2), with only a nine-centimetre gap, and correlates in the stratigraphy more effectively with the Unit 6 flowstone separating the samples in the profile (Spec18-5 & Spec18-4) (Fig 6; Fig. 7). Between the techniques applied to the sediments both SG-OSL and TT-OSL generally resulted in an agreement of ages that sit slightly younger than the expected range.

Methodology of OSL procedures was evaluated through a comparison of multigrain (MG), single grain (SG) and thermally transferred (TT) OSL techniques for accuracy and reliability of method. MG-OSL gave a temperature of 200°C for use in further SG determinations (Fig. 3), common for Australian quartz, to achieve the most reliable return signal (Fitzsimmons, 2011; Murray & Wintle, 2000). Dose recovery tests (DRTs) for Spec18-4 (OSL) (Table S1) and Spec18-2 (TT-OSL) (Table S2) and their radial plots (Fig. S3) are provided in supplementary information (SI). Alternatives of 160°C or 220°C may have been more suitable, and given a better signal response, as both temperatures also sit within the range of acceptability (Fig. 3). Australian quartz sediments and their dating limits are one of the current areas under investigation (Fitzsimmons, 2011).

MG-OSL is a mix of grains on a disc with no set quantity and calculates an average of all signals produced for a given spot size. Super grains or feldspars (bright signals) will skew the data to a higher age result, whereas saturated grains will not provide their true value and skew to a lower age (Arnold, Demuro, & Ruiz, 2012). These grain diversities may balance each other but are only an approximation of age with a larger error attributed (Arnold et al., 2012). SG-OSL pushed the limits of OSL dating (Rhodes, 2011; Murray & Wintle, 2000), with high numbers of saturated grains occurring, however, TT-OSL, a novel method used to extend the dating age range of (quartz) grains (Wang, 2006), proved useful in the cave setting being explored. Luminescence dating limits are being extended as improvements are made to the various techniques.

Variation in individual grain signals resulted in very high overdispersion (OD) of D_e values. High rejection rates occurred across all samples in both SG-OSL and TT-OSL methods, with a large number of saturated grains (1-4%) particularly within the deeper sediment layers. Overall the percent of accepted grains for each method ranged from 6-11% for OSL (Table S3) and 3-6% for TT-OSL (Table S4). Generally, there is a lower acceptance rate in TT-OSL

as the technique loses more grains to the rejection criteria (Table S4). Slow grains were another major factor in rejection of the quartz tested. A series of super grains with very large (irradiation) signal trapping capacity were also noted. All of the variation in signals and rejection of grains can be explained by the mixing of the cave sediments, transportation changes (affecting bleaching expectations), and a variety of source materials.

Bleaching expectations of how well sediments were bleached, or the length of exposure to sunlight of grains, can be assessed through its morphology (Murray & Olley, 2002). Well-rounded or well-worn grains indicate more exposure to sunlight, and therefore a greater chance of bleaching is more likely to have occurred (Murray & Olley, 2002). A retained or residual luminescence signal, from a lack of bleaching, influences D_e values and dating results (Arnold & Demuro, 2019; Murray & Olley, 2002). Younger grains are more likely to be fully bleached from same sediment profile (as older grains) and to not have reached saturation. Due to grain rejection leaving low numbers of D_e values, and high OD in those results, the MAM proved statistically sounder than CAM to use for the numerical dating (Wallinga & Cunningham, 2015).

Individual grain outputs displayed broadly scattered results indicating a mixed assortment of single grains with large errors for each. Radial plots (Fig 4) produced for all samples were based on 20% OD (Wallinga & Cunningham, 2015) using the MAM. High rejection rates of grains from saturation and slow luminescence signal were common across all five samples for a number of reasons including; from lack of bleaching (retention of signal); few trap spaces available (saturation or low capacity); and poor conditions conducive to signal retention or attraction. Based on the MAM output, SG-OSL dates attained compared to the TT-OSL dates returned established the later novel method to be quite reliable. The MAM model, although based on the younger ages, is more reliable as it ensures the most well bleached (younger) grains are the focus of the numerical age output. Further analysis of

grains for more D_e values should reduce OD, fine-tuning the age output and reducing the

error margins. Sediment transportation and deposition systems relate to the expected

bleaching levels of grains.

Sediments

Sediment conditions of transport to, and into, the cave, as well as storage (deposition) play a

part in the reliability of ages. Sediment transport to the cave was through several different

mechanisms; aeolian; fluvial; colluvial; or carried by local fauna. Distances travelled affect

the likelihood of grains being exposed to sunlight and reset prior to deposition into a cave.

Aeolian transported grains are the most likely to be fully bleached, being openly exposed to

sunlight, whereas fluvial borne grains may not have been completely exposed to sunlight as

water attenuates the light.

The external morphology of individual grains of sediment, such as, angularity, sphericity and

surface patterns, can be used to infer the conditions of transport. External conditions can also

indicate the phase of weathering between older, more worn grains to those freshly exposed.

Scanning electron microscope (SEM) images of cave quartz grains, display a mix of grain

shapes and surface textures (topography) (Fig. 10). The range of grain shapes are a mixture of

well-rounded, spherical (equant) and elongate, sub-rounded to sub-angular forms,

representing 'beach' sands, and, dunes, glacial till, or freshly weathered material sourced

from close by. Surface textures display wear patterns of v-shaped pock marks on spherical

grain surfaces (Fig. 10b), and elongate grains with conchoidal fracture patterns (Fig. 10c),

both a consequence of collisions which are consistent with an aeolian (secondary) transport

process (Darrénougué et al., 2009; Vos, et al., 2014). Secondary transport indicates a change

in environment and transport mode, for example, from coastal wash (well-rounded grains) to

aeolian carried material (v-shaped pock marks), until deposition as cave sediments. SEM

images also display more local and less travelled grain types indicating close proximity to the source materials (Vos et al., 2014).

The type of sediments that enter the cave are governed by several factors, including transport method, cave entrance type, climate and prevailing conditions. Sediments most commonly enter the cave system by falling and being washed in by rain (fluids) through any number of open pitfall and/or pipe entrances. Mixing of the sediment occurs as a part of this process, leaving an assorted sediment pile that may be further disturbed. Further movement (localised transport) of sediments, once in the cave, can occur from sediment passing the angle of repose (15°), mass movement down cone (gravity, creep), bioturbation (trapped fauna, termites), fluids (rainwater, groundwater), or even local fault movements (Sasowsky & Mylroie, 2007). Fine grain clays to coarse grain quartz all appeared well sorted, mature in texture and composition and in line with some of the other cave deposits in the Naracoorte Caves system (Forbes & Bestland, 2007). Maturity of the sediments is technically not very mature due to the high clay content. Although the sediments appear well sorted for their small size range, relevant to the cave environment, they are varied, with larger cave fragments interspersed (Fig 8; Table S6a, b; Fig S4). Kurtosis and skewness (average of all samples) presented a normal peak with a tail pull to the finer grain sizes (Fig. 9), along with a predominant 0.25 mm grain size, from the range analysed (Fig. 8). Due to the mechanisms of deposition in the cave setting and the entrance type the dominant 0.25 mm grain size was expected. In most Z-samples the small grain sizes of < 0.5 mm diameter made up over > 50% of the material (Fig. S4). Colour in the 5YR range mostly 4/6 or 5/6 in hue/chroma occurred in all four areas. Area 1-2 had predominantly yellowish-red with upper red-brown and sporadic reddish-yellow bands (Fig. 6; Fig. 7; Table S6a, b). Area 3-4 had predominantly reddish-yellow upper layers, interspersed with flowstone of green-grey-to dark brown, whilst lower in the profile was yellowish-red with a 10 cm wide section of closely spaced

flowstone-sediment layering (Fig. 6; Fig. 7; Table S6a, b). Red Brown Earths (RBEs), red bands of sediment with high iron content in the sediment layers, correlate with the RBE from the region (e.g. Coonawarra and Terra Rossa soils) (Barrie, 1997; Forbes & Bestland, 2007). Once in the cave system sediment deposition forms are not well sorted but a blend relevant to only smaller sizes (< 2 mm), with a mix of mineral types (mostly quartz and feldspar/clays), and minor quantities of clean sands, the remaining materials are varied, or in speleothem layers.

Sediment infill follows a similar input pattern to that found in the surrounding caves in the area. Sediment deposits are generally horizontal in nature with contacts between unconsolidated sediment layers not sharp; contact between unconsolidated sediments and flowstone deposits are sharp; and overall, hiatuses cannot easily be determined due to the mixed nature of the accumulations. Distinct banding in the sediments and some flowstone layers were used to arbitrarily denote Units, of which were further subdivided and sampled (Fig. 6, Fig. 7). Unit 6 (flowstone at 751 cm cave depth) is the only complete speleothem that crossed the 5 m wide space, creating a layer connection between all Areas, but tapers out in Area 1. Other flowstone layers either end abruptly, hit the cave wall, or abate somewhere between Areas 3-4 and Areas 1-2 (Fig. 2, cave map *r* to *u*).

Sediment overlay (Fig. 6) displays the unevenness of contacts between sediment units interspersed with flowstone, sand lenses and the gradual thinning of the Unit 6 flowstone layer. Lenses and wavy layers of sands may have filled previously disturbed spaces, be fluid escape structures, or, have been shifted or compacted by overburden of the overlying sediments as they accumulate. Some distinct sand lenses with very fine sands in Area 1-2 profile indicate a potential change of environment to drier conditions, or a wind shift bringing in materials from a different source.

Cave deposits are (reasonably) secure, compact, site histories from the surrounding region with the potential to identify lost surface formations (Smith, Bailey, Burgess, & Fraser, 2015). Cave sediment accumulation often occurs over multiple (continuous) deposition events, influenced by; timing of the opening/closing of cave entrance(s), especially open, for speleothem growth; changing cave shape through growth; the physical dynamics of entrance types; roof collapse(s) with boulders and rubble creating 'new' flooring, and; unconformities, particularly erosional surfaces. Understanding the cave sediment dynamics and infill sequence formation was used to infer past conditions.

Hiatuses (unconformities) are hard to determine in the depositional sequence in a cave setting due to mixing, resettling, material entry method and bioturbation. Unconformities are not clearly evident except where flowstone and sediments meet there is potential for a break in continuity of accumulation. A lack of sediment input during flowstone formation indicate wet conditions external to the cave as fluids are required for speleothem formation, and moist sediments are not easily shifted. Bimodal distribution establishes different entrances and sources and may not be evident if similar sediments are input through both (multiple) entrances from the same sources. Grain size analysis can be used to determine bimodal distribution. Size variation between the areas was not evident and no bimodal distribution was observed in the GSA for Specimen Cave.

Interspersed sediment deposition and solutional actions in the cave illustrates variation in local climate and/or weather conditions, including wind direction and fluid input. Wet and dry external conditions change the environment in the cave, with the former aiding speleothem growth and the latter allowing for increased sediment input. Sediment descriptions correlate with caves either side of the timeline suggesting continuity of deposits, and deposit sources, over the history sediment infill, however, geochemically there are differences.

Geochemistry

Geochemical methods of X-ray diffraction (XRD), X-ray fluorescence (XRF) and Itrax core

scanner (surface XRF) produced evidence of mineralogy and elemental composition of

materials that was both similar and different to the surrounding areas.

XRD

X-ray diffraction, for mineralogy, returned a significant amount of quartz in each of the

twelve Z-samples tested ranging from 77% to 90% (Fig. 11). The predominantly quartz

component would be partially controlled by the availability of source material in the areas

surrounding Specimen Cave, of which several stretches are palaeo-coastlines (Pedoja et al.,

2014) along with some glacial sediments (angular grains SEM, Fig. 10).

Referencing sediments of the Naracoorte Caves, surrounding areas, and wider regions,

examined by Forbes and Bestland (2007), Macken, et al. (2013), and Barrie (1997), found

that little correlation between these areas and other caves, to Specimen Cave, is evident.

Results from XRD (Fig. 11) of sediments from the cave were compared to the findings of

Forbes and Bestland (2007) with little correlation in mineralogy (except quartz) between the

caves (Grant Hall, Wet Cave, Robertson Cave and Fossil Chamber) temporally either side of

Specimen Cave. Mineralogy was also dissimilar to that of the surrounding (cave) sediments

and regional formations examined by Forbes and Bestland (2007) with Specimen Cave

lacking certain minerals, for example goethite and smectite. In place of goethite was hematite

as the iron bearing mineral and kaolinite, in place of smectite for clays were evident in most

samples (Fig. 11). Microcline was present in all samples along with calcite, of which much

was magnesium bearing (Fig. 11). Minor amounts of the minerals, albite, labradorite and

orthoclase are also present in nine, three and two samples respectively, covering the feldspars

and micas in the Z-samples (Fig. 11). Internally Z1 compared to Z14 establish the highest

correlation of overall mineralogy, both contain hematite and sit below Unit 6 in the stratigraphy (Fig 11; Fig. 7). Differences in the mineralogy of sediments conceivably indicate formations not yet analysed or missing (eroded) from the surrounding region(s).

XRF and ITRAX

Determination of elemental composition using surface XRF (Itrax) and bulk XRF methods, returned outcomes that were compared between methods where samples coincided at similar depths in stratigraphy.

Similarities in elemental composition was evident, and minor variations in results between the two methods at the same depth of sample occurred. Comparison sample matching of; Z-to Z-samples across Areas 1-2 and 3-4; and, Z-samples to Itrax depths (Fig 12 to Fig 14) down Area 1 (Fig. 7) were undertaken. Firstly, comparisons of Z8 to Z24, Z6 to Z22 and Z1 to Z14 as each set correlates across both areas for similar depth in profile (Fig, 7). Samples Z1 to Z14 show the highest correlation of elemental materials across the Areas and are below Unit 6 in the stratigraphy. XRF elements studied, seven of ten correlate between the Areas (Table 3), XRF oxides, nine out of twelve correlate between the Areas (Table 4). Secondly, comparisons of bulk XRF Z-samples to Itrax surface XRF core lengths exhibited variation in sediments indicating they were similar horizontally but not identical.

Individual Itrax sections display high iron content, indicating sediments from high iron containing source material, e.g. the Coonawarra RBEs, are evident at various depths (Barrie, 1997; Forbes & Bestland, 2007). Itrax, sections also consistently correlation low Si to high K, Ti, Mn, Fe, Sr; and, high Si to low Cl, K, Ca, Mn, Fe, Sr (Fig. 12, Fig. 13, Fig. 14) which requires further investigation (potential evaluation approaches see: Croudace & Rothwell, 2015).

Other materials established in the cave system were pollen, organics in general and megafaunal fossils. Fossils were present in small numbers but were avoided where possible in sample collection. Organic material was identified through LOI and Mo-ratio analysis (Dean 1974; Heiri et al., 2001; Croudace & Rothwell, 2015). Neither of these materials were examined in great detail.

The Itrax organic content was determined by the Mo (Inc/coh) with troughs matching low Si content (Fig. 12, Fig. 13, Fig. 14) (Croudace & Rothwell, 2015). LOI was used for determining organic content of individual bulk XRF samples using the methods of Dean (1974) and Heiri et al. (2001), returning organics between 2.80% and 7.21% per Z-sample (Table 4). Bulk XRF achieves higher sampling resolution than can be realized using the Itrax core surface scanner (Donaldson, 2016).

XRF elemental analysis (Table 5) returned reasonable consistency of elements between both areas horizontally within the cave. Differences in most individual element percentages (Table 5) were found when compared to similar data from nearby caves (Wet & Victoria Fossil) studied by Forbes and Bestland (2007).

Comparisons of individual (normalised) elements from the Itrax cores was commenced, with indicators of provenance and climate, K/Ti, producing an s-shaped plot, indicating changes to the aforementioned conditions (Fig. S5), and aeolian input, Si/Ti, with peaks signifying increased sediment input (Fig. S6) examined, further analysis can be done on these results (Croudace & Rothwell, 2015).

Palynology

The assay for pollen was negative in the four samples tested, suggesting either the cave conditions were not conducive to their preservation, or, very little to no particles entered the cave system, the former reason being the most likely (Hunt & Fiacconi, 2018). Pollen

particulates, collected in dolines around active cave entrances, would have eventually been

transported into the cave, but pollen requires anoxic conditions (when fluid is present) for its

preservation, which does not prevail in this cave setting (Hunt & Fiacconi, 2018).

Global Influences

Cave sediments examined sit between main dates of ~119 ka to ~166 ka which are extended

to ~107 ka and ~187 ka with tolerances. Unit 6 is constrained by ages of ~119 ka to ~142 ka

(Fig 15; Fig. 16). The dates specified coincide with mid MIS 6 through to MIS 5 (Fig. 15).

In general, global conditions during the aforementioned period observed; warmer

temperatures (1-2°C); increased carbon dioxide (CO_2) levels; increased water table levels; a

decrease in ice volume; lower dust levels; and, universal sea level rise (although localised sea

level regression-transgression cycles differ) (Fig. 16) (Pedoja et al., 2014). The sediment

deposition timing overlaps with the last interglacial ~130,000 years ago and ended ~115,000

years ago at the beginning of the last glacial period, lasting 15,000 years. Unit 6 occurs in the

MIS 5e stage, of increased water availability from low ice volume, coupled with sea level rise

and increased CO_2, which allows for increased speleothem production (Pedoja et al., 2014).

Speleothem production, from increased fluids and CO_2 in the cave system altering calcium

carbonate ($CaCO_3$) to carbonic acid (H_2CO_3), which further dissolves the cave limestone,

until degassing (CO_2) occurs, with fine grained flowstone laminae being deposited (Webb, et

al., 2003). The banded nature of the laminae discloses separate formation events over the

cave history with wetter conditions occurring simultaneously (Fairchild, 2013). Degassing

also contributes to additional CO_2 in the atmosphere, whereas speleothem production

increases from CO_2 presence in the right conditions.

The conditions in the cave related to the external environment appear to be different to that of

the surrounding caves, in that there were increased sea levels affecting water table heights,

increased temperatures and CO_2 levels (Pedoja et al., 2014). Low dust concentrations indicating a wetter climate, with less material input into the cave system, coincide with speleothem production. Continental uplift may have also affected the conditions related to the cave sediment input (Pedoja et al., 2014).

These outcomes are important to the understanding of current climate change; since global mean temperatures during MIS-5e are similar to the projected climate change of today, and its effects on nature over the same timeframe; with past extinction factors, along with species types and numbers, relating to the extinction of current species from those (similar) climate changes.

CONCLUSIONS

A digitised cave map for the relative sections of Specimen Cave relevant to the sampling locations was completed.

Luminescence dating of the sediments provided constraint on the encompassed megafaunal inclusions to between 119.27 ± 13.50 ka to 156.49 ± 12.67 ka for OSL, and for TT-OSL, to between 141.94 ± 24.12 ka and 165.50 ± 21.19 ka using MAM. Single grained OSL method provided better outcomes for the type of sediment accumulation than multi-grained analysis. The TT-OSL dating method provided better results for the age extent of sediments than single grained OSL analysis and proved a reliable method for Middle Pleistocene sediments. The most reliable OSL technique was TT-OSL because SG-OSL had reached its limits of dating of the cave sediments due to grain saturation. Dates were affected by high rate of rejected grains and possibly underrepresented in older grains due to saturation.

Sediments were consistent with aeolian, fluvial and colluvial input. Sediment provenance was not determined through comparative analysis with other local sediment descriptions, but further sampling from surrounding areas may elucidate their origins.

XRD results correlate in cave, but differences between surrounding caves are evident. XRF

and ITRAX results display interesting parallels that can be further investigated. Very little

organic material was present in the cave samples and all were negative for pollen. Sediment

analysis indicates mixing of grains, which affects how well (age) dating performs in the areas

of bleaching expectations, from transport and storage conditions

These findings relate to current climate change, as global mean temperatures during MIS-5e

are considered similar to expected climate changes.

REFERENCES

AITKEN, M.J. (1998). An Introduction to Optical Dating: The Dating of Quaternary Sediments by the Use of Photon-Stimulated Luminescence. Oxford University Press, Oxford, 267.

ARNOLD, L. J., DEMURO, M., & RUIZ, M. N. (2012). Empirical insights into multi-grain averaging effects from 'pseudo' single-grain OSL measurements. *Radiation Measurements, 47*(9), 652-658. doi:10.1016/j.radmeas.2012.02.005.

ARNOLD, L. J., DUVAL, M., FALGUÈRES, C., BAHAIN, J. J., & DEMURO, M. (2012). Portable gamma spectrometry with cerium-doped lanthanum bromide scintillators: Suitability assessments for luminescence and electron spin resonance dating applications. *Radiation Measurements, 47*(1), 6-18. doi:10.1016/j.radmeas.2011.09.001.

BARRIE, J. (1997). Climatic indicators within Henschke fossil cave system, Naracoorte, South Australia. *Quaternary Australasia, 15*(2), 45-57.

BOGGS, S. (2009). *Petrology of sedimentary rocks* (2nd ed. ed.). Cambridge: Cambridge University Press.

BOGGS, S. J. (2014). *Principles of sedimentology and stratigraphy* (Fifth edition. ed.): Pearson.

CHAPOT, M. S., ROBERTS, H. M., LAMB, H. F., SCHÄBITZ, F., ASRAT, A., TRAUTH, M. H., & THE CHEW BAHIR SCIENCE TEAM. (2017). Defining the upper age limit of luminescence dating: A case study using long lacustrine records from Chew Bahir, Ethiopia. *Geophysical Research Abstracts, 19*(EGU2017-18159, 2017).

CROUDACE, I. W., RINDBY, A., & ROTHWELL, R. G. (2006). ITRAX: description and evaluation of a new multi-function X-ray core scanner. *Geological Society, London, Special Publications, 267*(1), 51-63. doi:10.1144/gsl.sp.2006.267.01.04.

CROUDACE, I. W., & ROTHWELL, R. G. (2015). *Micro-XRF Studies of Sediment Cores Applications of a non-destructive Tool for the Environmental Sciences.* (Vol. 17).

DAHL-JENSEN, D., ALBERT, M. R., ALDAHAN, A., AZUMA, N., BALSLEV-CLAUSEN, D., BAUMGARTNER, M., . . . GOTO-AZUMA, K.; ET AL. (2013). *"Eemian interglacial reconstructed from a Greenland folded ice core". Nature. 493 (7433): 489–94.* doi:10.1038/nature11789.

DARRÉNOUGUÉ, N., DE DECKKER, P., FITZSIMMONS, K. E., NORMAN, M. D., REED, L., VAN DER KAARS, S., & FALLON, S. (2009). A late Pleistocene record of aeolian sedimentation in Blanche Cave, Naracoorte, South Australia. *Quaternary Science Reviews, 28*(25-26), 2600-2615. doi:10.1016/j.quascirev.2009.05.021.

DEAN, W.E. (1974). Determination of carbonate and organic matter in calcareous sediments and sedimentary rocks by loss on ignition: comparison with other methods. *Journal of Sedimentary Research* 44, 242–248.

DEPARTMENT FOR ENVIRONMENT AND HERITAGE (2001). *Naracoorte Caves National Park Management Plan.* (ISBN 0 7308 5846 4). South Australia.

DONALDSON, G. M. (2016). *1931-Waikari-River-Tsunami-New-Zealands-largest-historical-tsunami.* (Bachelor of Science (Honours)), New South Wales.

DULLER, G.A.T. (2015). The Analyst software package for luminescence data: overview and recent improvements. Ancient TL 33, 35-42.

FAIRCHILD, I. (2013). Cave deposits (speleothems) as archives of environmental change. *Climatica.*

FITZSIMMONS, K. (2011). An Assessment of the Luminescence Sensitivity of Australian Quartz with respect to Sediment History. *Geochronometria, 38*(3), 199-208. doi:10.2478/s13386-011-0030-9.

FORBES, M. S., & BESTLAND, E. A. (2006). Guano-derived deposits within the sandy cave fills of Naracoorte, South Australia.

FORBES, M. S., & BESTLAND, E. A. (2007). Origin of the sedimentary deposits of the Naracoorte Caves, South Australia. *Geomorphology, 86*(3-4), 369-392. doi:10.1016/j.geomorph.2006.09.009.

FORBES, M. S., BESTLAND, E. A., WELLS, R. T., & KRULL, E. S. (2007). Palaeoenvironmental reconstruction of the Late Pleistocene to Early Holocene Robertson Cave sedimentary deposit, Naracoorte, South Australia. *Australian Journal of Earth Sciences, 54*(4), 541-559. doi:10.1080/08120090601078388.

GRIMES, K. (1997). ASF Cave Survey and Map Standards by Edward G. Anderson and others, 1978, ASF Survey Commission.

GRIMES, K. G., & WHITE, S. Q. (2004). Geological Development of the Naracoorte Caves, South Australia. *Helictite, 39*(2), 55-75.

HEIRI, O., LOTTER, A.F., LEMCKE, G. (2001). Loss on ignition as a method for estimating organic and carbonate content in sediments: reproducibility and comparability of results. *Journal of Paleolimnology* 25, 101-110.

HUNT, C. O., & FIACCONI, M. (2018). Pollen taphonomy of cave sediments: What does the pollen record in caves tell us about external environments and how do we assess its reliability? *Quaternary International, 485*, 68-75. doi:10.1016/j.quaint.2017.05.016.

KELTS, K. (1998). Components In lake sediments: smear slide identifications, LRC Core Facility, The University of Minnesota.

LAUER, T., & WEISS, M. (2018). Timing of the Saalian- and Elsterian glacial cycles and the implications for Middle – Pleistocene hominin presence in central Europe. *Scientific Reports, 8*(1), 5111. doi:10.1038/s41598-018-23541-w.

LEWIS, I. D. (2017). *Summary of State Heritage Place: 26459 Naracoorte Caves Complex*. South Australia.

LINNENLUCKE, L. P. (2012). *Single-grain optically stimulated luminescence (OSL) dating of terminal Pleistocene and early Holocene human occupation sites in the Dhofar region of Oman.* (Bachelor of Science (Honours), School of Earth & Environmental Science, Honours), University of Wollongong, Retrieved from http://ro.uow.edu.au/thsci/61.

LISIECKI, L. E., & RAYMO, M. E. (2005). A Pliocene-Pleistocene stack of 57 globally distributed benthic δ18O records. *Paleoceanography, 20*(1-17). doi:10.1029/2004PA001071.

MACKEN, A. C., JANKOWSKI, N. R., PRICE, G. J., BESTLAND, E. A., REED, E. H., PRIDEAUX, G. J., & ROBERTS, R. G. (2011). Application of sedimentary and chronological analyses to refine the depositional context of a Late Pleistocene vertebrate deposit, Naracoorte, South Australia. *Quaternary Science Reviews, 30*(19-20), 2690-2702. doi:10.1016/j.quascirev.2011.05.023.

MACKEN, A. C., MCDOWELL, M. C., BARTHOLOMEUSZ, D. N., & REED, E. H. (2013). Chronology and stratigraphy of the Wet Cave vertebrate fossil deposit, Naracoorte, and relationship to paleoclimatic conditions of the Last Glacial Cycle in south-eastern Australia. *Australian Journal of Earth Sciences, 60*(2), 271-281. doi:10.1080/08120099.2013.758657.

MURRAY, A. S., & OLLEY, J. M. (2002). Precision and Accuracy in the Optically Stimulated Luminescence Dating of Sedimentry Quartz: A Status Review. *Journal on Methods and Applications of Absolute Chronology. Geochronometria, 21*, 1-16.

MURRAY, A. S., & WINTLE, A. G. (2000). Luminescence dating of quartz using an improved single aliquot regenerative-dose protocol. *Radiation Measurements*(32), 57-73.

NGUYEN, N., et. al. (c2013). Palynology and Geochemistry Data And Methods, and Section Age Model: Supplementary Information.

PEDOJA, K., HUSSON, L., JOHNSON, M. E., MELNICK, D., WITT, C., POCHAT, S., . . . GARESTIER, F. (2014). Coastal staircase sequences reflecting sea-level oscillations and tectonic uplift during the Quaternary and Neogene. *Earth-Science Reviews, 132*, 13-38. doi:10.1016/j.earscirev.2014.01.007.

PETIT, J. R., JOUZEL, J., RAYNAUD, D., BARKOV, N. I., BARNOLA, J. M., BASILE, I., . . . STIEVENARD, M. (1999). Climate and atmospheric history of the past 420,000 years from the Vostok ice core, Antarctica. *Nature, 399*, 429. doi:10.1038/20859.

PRESCOTT, J.R., HUTTON, J.T. (1994). Cosmic ray contributions to dose rates for luminescence and ESR dating: large depths and long-term time variations. *Radiation Measurements* (230, 497-500.

RAILSBACK, L. B., GIBBARD, P. L., HEAD, M. J., VOARINTSOA, N. R. G., & TOUCANNE, S. (2015). An optimized scheme of lettered marine isotope substages for the last 1.0 million years, and the climatostratigraphic nature of isotope stages and substages. *Quaternary Science Reviews, 111*, 94-106. doi:https://doi.org/10.1016/j.quascirev.2015.01.012.

REED, E. H., & BOURNE, S. J. (2000). Pleistocene Fossil Vertebrate Sites Of The South-East Region Of South Australia. *Transactions of the Royal Society of South Australia, 124*(2), 61-90.

ROHDE, R. A. (c2008). Ice Age Temperature Changes graph, University of California, Berkeley.

RHODES, E. J. (2011). Optically Stimulated Luminescence Dating of Sediments over the Past 200,000 Years. *Annual Review of Earth and Planetary Sciences, 39*(1), 461-488. doi:10.1146/annurev-earth-040610-133425.

ROHLING, E. J.; GRANT, K.; HEMLEBEN, CH.; SIDDALL, M.; HOOGAKKER, B. A. A.; BOLSHAW, M.; KUCERA, M. (2007). High rates of sea-level rise during the last interglacial period. *Nature Geoscience.* 1: 38–42. doi:10.1038/ngeo.2007.28.

SASOWSKY, I. D., & MYLROIE, J. (2007). *Studies of Cave Sediments Physical and Chemical Records of Paleoclimate*: Springer Netherlands. p23-44.

SMITH, D. G., BAILEY, R. J., BURGESS, P. M., & FRASER, A. J. (2015). *Strata and time : probing the gaps in our understanding.* The Geological Society, London, p 242.

VOS, K., VANDENBERGHE, N., & ELSEN, J. (2014). Surface textural analysis ofquartz grains by scanning electron microscopy (SEM): From sample preparation to environmental interpretation. *Earth-Science Reviews*(128), 93-104. doi:10.1016/j.earscirev.2013.10.013.

WALLINGA, J., & CUNNINGHAM, A. C. (2015). Luminescence Dating, Uncertainties and Age Range. In *Encyclopedia of Scientific Dating Methods* (pp. 440-445).

WANG, X. L., WINTLE, A. G., & LU, Y. C. (2006). Thermally transferred luminescence in fine-grained quartz from Chinese loess: Basic observations. *Radiation Measurements*(41), 649-658. doi:10.1016/j.radmeas.2006.01.001.

WEBB, J., GRIMES, K., & OSBORNE, A. (2003). Black Holes: caves in the Australian landscape In B. Finlayson & E. Hamilton-Smith (Eds.), *Beneath the Surface: a natural history of Australian caves.* (pp. 1-52). Sydney: University of New South Wales Press.

WEI, G., LIU, Y., LI, X., SHAO, L., & LIANG, X. (2003). Climatic impact on Al, K, Sc and Ti in marine sediments: Evidence from ODP Site 1144, South China Sea. *Geochemical Journal, 37*, 593-602.

WHITE, S. Q., & WEBB, J. A. (2015). The influence of tectonics on flank margin cave formation on a passive continental margin: Naracoorte, Southeastern Australia. *Geomorphology, 229*, 58-72. doi:10.1016/j.geomorph.2014.09.003.

WOOKEY, ATKINSON, A., & DAY, A. (1995). Expedition Surveying Guide, Cambridge University Caving Club, [accessed March 2018] <https://www.sat.dundee.ac.uk/~arb/speleo/gpfseminar96/survey.html>.

ZANDER, A., & HILGERS, A. (2013). Potential and limits of OSL, TT-OSL, IRSL and pIRIR$_{290}$ dating methods applied on a Middle Pleistocene sediment record of Lake El'gygytgyn, Russia. *Climate of the Past, 9*(2), 719-733. doi:10.5194/cp-9-719-2013.

SUPPLEMENTARY INFORMATION

Site
Cave Mapping
The cave was remapped by hand using a Lecia laser range finder centre line walk-and-measure method; hand mapping by walking a central line, taking measurements Right hand side (RHS), Left hand side (LHS), floor to roof (up, down) [LRUD], and end to end, for complete width and length of cave and lower cave spaces (L. Reed pers. comm. April 2018; Wookey, Atkinson, and Day,1995).
Digitising the map of cave parameters for layout and profile of upper and lower cave areas combined with outlining and adjustment of a scanned copy of the original 1959 map CEG 1119, from the Cave Exploration Group (CEG) (App. A Fig S1) using CorelDRAW© Home and Student 2018.
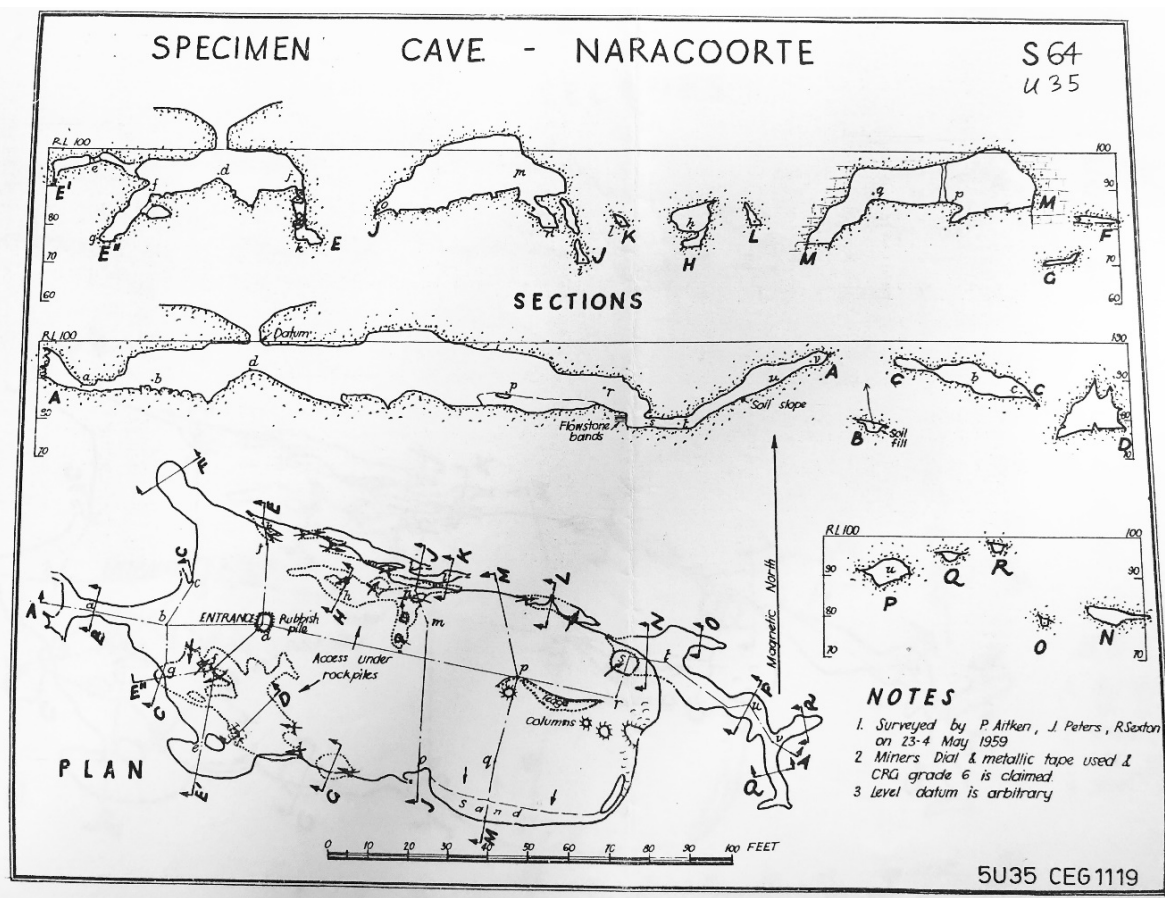
Figure S1. Scanned copy of the original Specimen Cave map, 5U35 CEG 1119.

Photogrammetry
Photographic records, carried out before, during and after sample collection, were taken on a Sony Cybershot DSC-TX230 18.2-megapixel camera and modified using editing software, Microsoft Paint© and CorelDRAW©. A further 364 photographs were taken to produce a 3D composite image (photogrammetry) and correlated using Agisoft© software. The photos overlap by ~80% vertically and ~40% horizontally and are joined to create a composite 3D image of sediment surface.
Sample Collection
In the lower section of the cave, after removal of loose overburden, excavation was carried out removing excess sediments to expose a clean deposit. Five samples (Spec18-1 to Spec18-

5) in 50 mm tubes were obtained from the sediment cone for dating, and were sealed from light exposure. Each sample space had a further 100 mm sediment collected that was encircling the original sample for dosimetry, water and moisture content testing and were sealed from moisture loss. Spacing was set out with a minimum of 30 cm of sediment in all directions from each sample collected (Fig. S2).
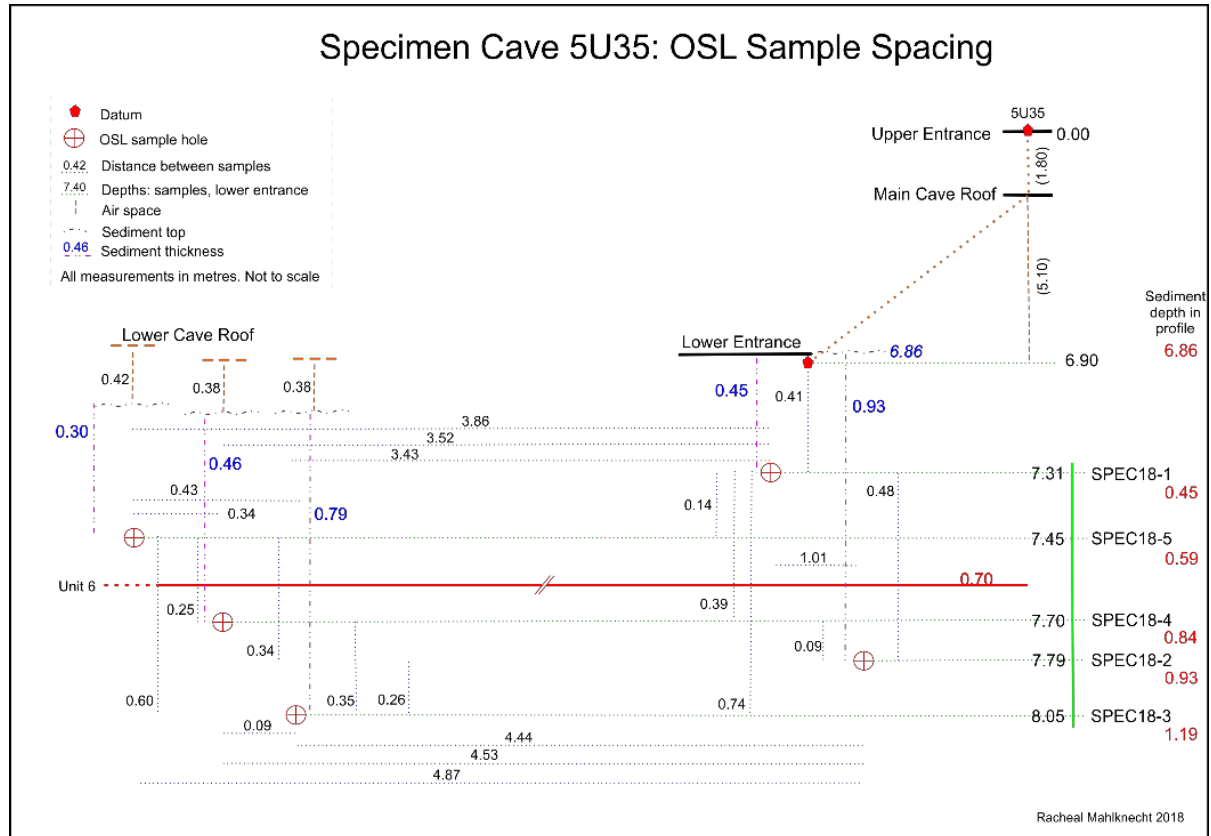
Figure S2. Depths and distances of sample spacing for luminescence dating **Figure S2**: Specimen Cave OSL sample spacing. Distances in between each OSL sample and the surrounding cave, including roof heights and air spaces for dose rate calculations. Lower cave section facing 204° SSW (Mahlknecht, R., 2018).

Luminescence
Sample Preparation and Rejection Criteria
All luminescence samples were prepared, analysed and are stored at Prescott Environmental Luminescence Laboratory (PELL), University of Adelaide**,** under dark (red) lighting conditions.

Preparation of five sediment samples (Spec18-1 to 5) was completed with each sample tube opened and the ends discarded, in 5 mm step stages to a 2 cm depth, to ensure any light exposed grains were removed. Each sample was wet sieved with the 212-250 μm fraction then treated with 10% HCl (40 mins) and 30% H_2O_2 (overnight) to remove carbonates and organic material. Density separation of the dried samples, using lithium heteropolytungstate (LST), with the quartz fraction then etched with hydrofluoric acid, oven dried, and dry sieved, with the 125-180 μm quartz fraction utilised for equivalent dose estimation and dating experiments (Linnenlucke, 2012; Aitken, 1998, with variations).

Of the extra sediments surrounding the main sample both saturated water and moisture content (effective water content) were determined (Table S5). The remaining material was dried, homogenised (Retsch PM100 ball mill) and prepared for gamma-ray spectrometry and beta dose determination which was assessed in laboratory (Table S5). In situ and in

laboratory dosimetry measurements were combined with cosmic-ray estimate, following Prescott and Hutton (1994), and used for age calculations (Table S5).

Samples were loaded onto standard single-grain aluminium discs (300 μm x 300 μm, with an array of 100 drilled holes).

All dose determination sets were performed on Riso 2. Sample preparation via the methods outlined by Aitken (1998), for OSL dating, and Wang et.al., (2006) for TT-OSL with variations based on sample outputs from DRTs. Summary results for the SAR protocols, based on Murray and Wintle (2000), and Arnold et al. (2018), are in Tables S1 to S4 and the rejection criteria are as follows:

Single-grain OSL D_e estimates were rejected from further consideration if they exhibited one or more of the following properties:

 (i)   weak OSL signals
 (ii)   slow signals
 (iii)   poor recycling ratios
 (iv)   saturated or non-intersecting natural OSL signals
 (v)   anomalous dose-response curves; zero or negative response with increasing dose; very scattered L_x/T_x values
 (vi)   high levels of signal recuperation / charge transfer between SAR cycles
 (vii)   contamination by inclusions or feldspar grains

Additional information for age determination: Cosmic-ray dose rates using the equations of Prescott and Hutton (1994) were calculated with considerations to geomagnetic latitude, site altitude, and thickness of the sediment overburden in the area of interest.

Individual grain analysis was performed using Analyst v3.14© (Duller, 2015) and SAR Rejection Criteria spreadsheets, with modifications from daily beta dose adjustment sheets and grain position spatial adjustment calibration sheets (all Microsoft Excel© spreadsheets supplied by L. Arnold, pers. comm. 2018).

The general age equation:

$$Age \ (ka) = \frac{Equivalent \ Dose \ (Gy)}{Environmental \ Dose \ Rate \ (Gy/ka)} \qquad \textbf{eq 1}$$

Where the equivalent dose (D_e) (eq 1) or palaeodose, is measured in Grey (Gy), and the environmental dose rate (D_r) in Grey per thousand years (Gy/ka), was used to calculate numerical ages.

Luminescence DRTs

Underrepresentation in older grains causes skewing of the determined age to younger values.

Table S1. Summary data – DRT for OSL grain size 212-250 μm statistics exhibiting proportion of rejected and accepted grains after applying the SAR rejection criteria.

Sample	SPEC18-4_DRT		SPEC18-4 DRT2	
OSL DRT	**Number**	**%**	**Number**	**%**
Total No. grains	400	100	200	100
Grains rejection criteria				
Nat <3sigma BG	120	30	91	46
Poor Low R ratio	51	13	18	9
Poor High R ratio	28	7	10	5
Depletion by IR	14	4	7	4
Recuperation >5%	2	1	0	0
Non-intercepting grains	43	11	0	0
Extrapolated grains	2	1	0	0
Saturated grains	8	2	0	0
Anomalous dose response curve / poor fit	56	14	52	26
Sum of rejected grains	**324**	**81**	**178**	**89**
Sum of accepted grains	**76**	**19**	**22**	**11**

Table S2. Summary data – DRT for TT-OSL grain size 212-250 μm statistics exhibiting proportion of rejected and accepted grains after applying the SAR rejection criteria.

Sample	SPEC18-2 DRT	
TT-OSL DRT	**Number**	**%**
Total No. grains	500	100
Grains rejection criteria		
Nat <3sigma BG	338	67
Poor Low R ratio	37	7
Depletion by IR	0	0
Recuperation >5%	0	0
Non-intercepting grains	6	1
Extrapolated grains	1	0
Saturated grains	14	3
Anomalous dose response curve /poor fit	83	17
Sum of rejected grains	**479**	**96**
Sum of accepted grains	**21**	**4**

Table S3. Summary data – OSL grain size 212-250 μm statistics exhibiting proportion of rejected and accepted grains after applying the SAR rejection criteria.

Sample	SPEC18-1		SPEC18-2		SPEC18-3		SPEC18-4		Spec18-5	
OSL	**Number**	**%**	**Number**	**%**	**Number**	**%**	**Number**	**%**	**Number**	**%**
Total No. grains	800	100	800	100	800	100	800	100	1000	100
Grains rejection criteria										
Nat <3sigma BG	310	39	410	51	417	52	385	48	443	44
Poor Low R ratio	108	14	76	10	100	13	88	11	127	13
Poor High R ratio	70	9	72	9	72	9	74	9	78	8
Depletion by IR	17	2	31	4	25	3	19	2	30	3
Recuperation >5%	8	1	5	1	9	1	3	0	6	1
Non-intercepting grains	66	8	57	7	56	7	60	8	87	9
Extrapolated grains	0	0	1	0	0	0	0	0	1	0
Saturated grains	17	2	12	2	11	1	30	4	26	3
Anomalous dose response curve / poor fit	127	16	134	17	140	18	183	23	238	24
Sum of rejected grains	**723**	**90**	**709**	**89**	**727**	**91**	**744**	**93**	**937**	**94**
Sum of accepted grains	**77**	**10**	**91**	**11**	**73**	**9**	**56**	**7**	**63**	**6**

Table S4. Summary data –TT-OSL grain size 212-250 μm statistics exhibiting proportion of rejected and accepted grains after applying the SAR rejection criteria.

Sample	SPEC18-2		SPEC18-3		SPEC18-4	
TT-OSL	**Number**	**%**	**Number**	**%**	**Number**	**%**
Total No. grains	800	100	1000	100	800	100
Grains rejection criteria						
Nat <3sigma BG	485	61	685	69	529	66
Poor Low R ratio	62	8	82	8	50	6
Depletion by IR	0	0	0	0	0	0
Recuperation >5%	0	0	0	0	0	0
Non-intercepting grains	6	1	6	1	1	0
Extrapolated grains	0	0	0	0	0	0
Saturated grains	27	3	16	2	9	1
Anomalous dose response curve /poor fit	175	22	228	23	183	23
Sum of rejected grains	**755**	**94**	**969**	**97**	**772**	**97**
Sum of accepted grains	**45**	**6**	**31**	**3**	**28**	**4**
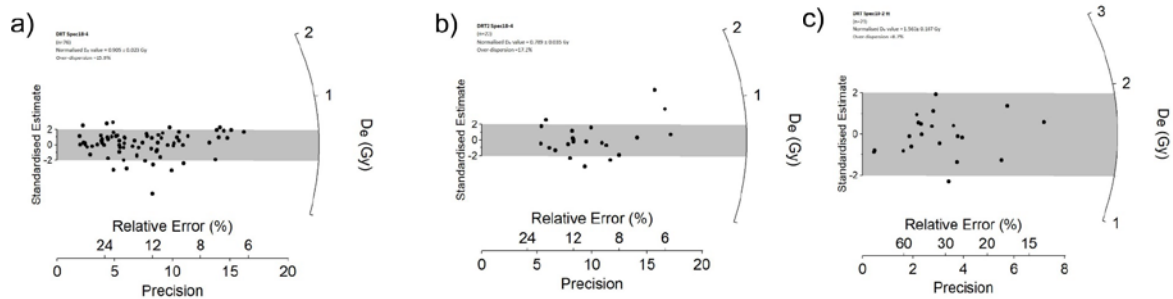
Figure S3. Radial Plots for DRTs. a) & b) Spec18-4 two trials (400 and 200 grains respectively per trial) SG-OSL and c) Spec18-2 TT-OSL.

Table S5. Spec18 sample dosimetry and water content. (*TBA to be added*)

Sample	Sample depth (cm)	Water content [a]	Grain fraction (μm)	Gamma dose rate (Gy/ka) [b, c] TBA	Beta dose rate (Gy/ka) [d]	Cosmic dose rate (Gy/ka) [e]	Internal dose rate (U+Th) (Gy/ka) [f] TBA	Total dose rate (Gy/ka) [g] TBA
Spec18-1	731	25.7	212-250	0.00±0.00	0.18±0.01	0.058±0.006	0.00±0.00	0.00±0.00
Spec18-2	779	27.5	212-250	0.00±0.00	0.29±0.02	0.058±0.006	0.00±0.00	0.00±0.00
Spec18-3	805	27.6	212-250	0.00±0.00	0.21±0.01	0.058±0.006	0.00±0.00	0.00±0.00
Spec18-4	770	27.5	212-250	0.00±0.00	0.35±0.02	0.058±0.006	0.00±0.00	0.00±0.00
Spec18-5	745	26.3	212-250	0.00±0.00	0.35±0.02	0.058±0.006	0.00±0.00	0.00±0.00

a Water content, expressed as % of dry mass of sample and assigned a relative uncertainty of ± 20%.

b TBA

c TBA

d Beta dose rates were determined using a Risø GM-25-5 low-level beta counter (Bøtter-Jensen and Mejdahl, 1988), after making allowance for beta dose attenuation due to grain-size effects and HF etching (Brennan, 2003).

e Cosmic-ray dose rates were calculated following Prescott and Hutton (1994) and assigned a relative uncertainty of ± 10%.

f TBA

g TBA

Sedimentology

Sediment

Full sediment descriptions of each of the 90 laminae are included in Tables S6a and b and indicate both profile depth and thickness of each one. Samples are stored at PELL at the University of Adelaide.

Descriptions included sorting, texture, composition (QFL%), maturity, sizing and colour were carried out using a 10x and 40x hand lens in natural sunlight (Table S6a, b).

The colour descriptions were based on the Munsell Colour Chart (2016) and performed in natural sunlight between 10 am and 2 pm over 2 days. The stratigraphic log was recorded in Microsoft Excel©, compiled in SedLog v3.1©, and edited in CorelDRAW© 2018.

SEM, mounting of samples onto 12 mm Al-metal 'pins', with a flat top and an attached carbon sticky pad, were dipped into sediments for an even coating and tapped to remove excess material then coated with 5 nm layer of platinum for high resolution imaging (D. Kelsey, pers. comm. 2018).

Smear slides

Smear slides for petrography were prepared by placing a small sediment sample in ethanol on a slide, placing a cover slip on top and attaching with clear silicone to seal (Kelts, 1998) Slides made but not photographed or analysed as the silicone did not prevent the leaking of the ethanol. The use of optical cement for sealing the sediment is recommended.

GSA

Grain size analysis, was completed using Endicott 200mm diameter stacking sieves, sizes 500, 250, 125, 63, 38 μm, with receiver and lid, for collected fractions of <500, <250, <125, <63, <38, >38 μm. Each of the 12 samples selected were individually weighed and then sieved by hand (Table 2). After separation each fraction was weighed and then summed to compare to the original weight, for sample loss. The sieves were cleaned between each sample run. Grain size analysis particle fractions of seven samples, percentage of each sieved size for Area 1-2 (Fig. S3) and the sizes using the Wentworth-Uden scale percentage of each size (Table S7).
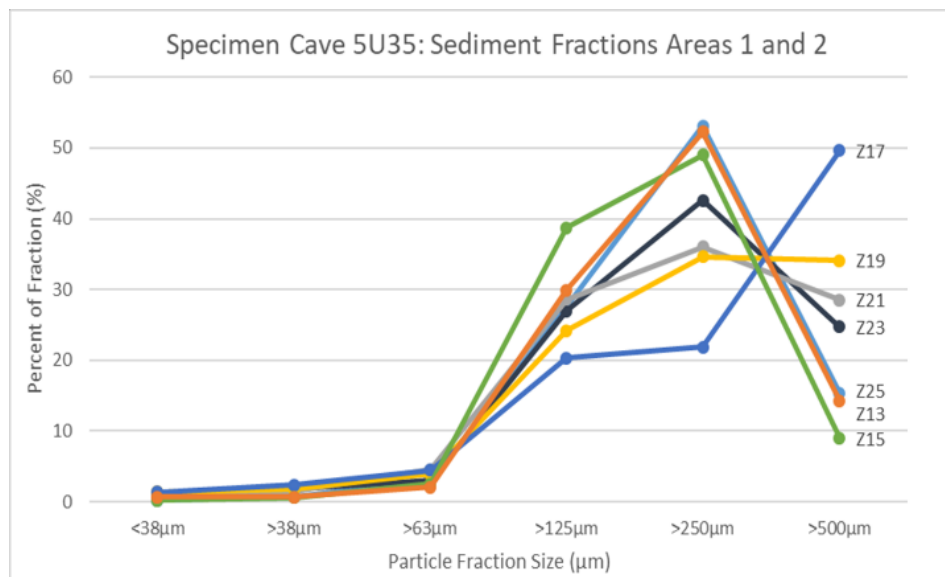
Figure S4. :Specimen Cave sediment grain (particle) size analysis. Sediments from adjacent sets, Area 1 and Area 2, display consistent grain size composition in each layer at depths ranging from 7.13 m (Z25) to 7.90 m (Z13). Sample Z17 Area 3-4 contained greater amounts of cave limestone and fossilised bone fragments – the only sample below 50% >500μm.

SEM

Micrographs of quartz grains and cave sediment from Secondary Electron (SE) and backscattered electron (BSE) were edited in Microsoft Paint© and CorelDRAW© 2018.

Table S6a. Area 1 and 2 sediments, individual grain descriptions for Specimen Cave.

number	profile Depth (cm)	thickness s (cm)	Area A	Unit U	No (Small) S	Colour Code	Colour Name	Shape Sphericity	Shape Angularity	Quartz	Feldsp	Lithics/calcite	Texture	Sorting	Maturity	cementation	Description
																	grain supported
1	-1	1	1	1	1	5YR 4/3	reddish brown	spherical	sub-angular	20	75	5	fine/med fine	well sorted	mature	uncnsld sedimemt	grain supported
2	0	1	1	1	2	5YR 4/6	yellowish red	spherical	sub-rounded	85	15	0	fine/med fine	well sorted	mature	uncnsld sedimemt	grain supported
3	1	1	1	1	3	5YR 4/6	yellowish red	spherical	sub-angular	70	25	5	fine/med fine	well sorted	mature	uncnsld sedimemt	grain sprtd. Charcoal frag. Bone
4	2	2.5	1	1	4	5YR 4/6	yellowish red	spherical	sub-angular	60	40	0	fine/med fine	well sorted	mature	uncnsld sedimemt	grain supported
5	4.5	3.5	1	1	5	5YR 4/4	reddish brown	spherical	sub-rounded	10	89	1	fine	well sorted	mature	uncnsld sedimemt	grain supported. L/stone flakes, Charcoal frag.
6	8	0.5	1	1	6	5YR 4/4	reddish brown	sph/elong	sub-ang/-rnd	10	89	1	fine/med fine	well sorted	mature	uncnsld sedimemt	grain supported
7	8.5	0.5	1	2	7	5YR 4/4	reddish brown	sph/elong	sub-ang/-rnd	10	89	1	fine/med fine	well sorted	mature	uncnsld sedimemt	grain supported, calcite
8	9	0.5	1	2	8	5YR 4/6	yellowish red	spherical	sub-angular	10	89	1	med fine	well sorted	mature	uncnsld sedimemt	grain supported
9	9.5	1	1	2	9	5YR 4/6	yellowish red	sph/elong	sub-angular	2	98		med fine	well sorted	mature	uncnsld sedimemt	grain supported
10	10.5	0.5	1	2	10	5YR 4/6	yellowish red	sph/elong	sub-angular	2	98		med fine	well sorted	mature	uncnsld sedimemt	grain supported
11	11	1.5	1	2	11	5YR 4/6	yellowish red	spherical	sub-angular	10	90		fine/med fine	well sorted	mature	uncnsld sedimemt	grain supported, bone
12	12.5	0.5	1	2	12	5YR 4/6	yellowish red	spherical	sub-rounded	10	90		fine/med fine	well sorted	mature	uncnsld sedimemt	grain supported, calcite
13	13	0.5	1	2	13	5YR 4/6	yellowish red	spherical	sub-rounded	10	90		fine/med fine	well sorted	mature	uncnsld sedimemt	grain supported
14	13.5	1.5	1	2	14	5YR 4/6	yellowish red	spherical	sub-angular	10	90		fine/med fine	well sorted	mature	uncnsld sedimemt	grain supported
15	15	1.5	1	2	15	5YR 4/6	yellowish red	spherical	sub-ang/-rnd	10	90		fine/med fine	well sorted	mature	uncnsld sedimemt	grain supported
16	16.5	0.5	1	2	16	5YR 4/6	yellowish red	spherical	sub-angular	10	90		fine/med fine	well sorted	mature	uncnsld sedimemt	grain supported, calcite
17	17	2.5	1	2	17	5YR 5/6	yellowish red	spherical	sub-angular	75	25		fine/med fine	well sorted	mature	uncnsld sedimemt	grain supported
18	19.5	1.5	1	2	18	5YR 5/6	yellowish red	spherical	sub-angular	95	5		med fine	well sorted	mature	uncnsld sedimemt	grain supported
19 [a]	21	9.5	1	3	19	5YR 4/6	yellowish red	spherical	sub-ang/-rnd	10	90		med fine	well sorted	mature	uncnsld sedimemt	grain supported
20	26	in above	1	3	20	5YR 4/6	yellowish red	spherical	sub-ang/-rnd	9	90	1	med fine	well sorted	mature	uncnsld sedimemt	grain supported
21	30.5	in above	1	3	21	5YR 4/6	yellowish red	spherical	sub-ang/-rnd	9	90	1	fine/med fine	well sorted	mature	uncnsld sedimemt	grain supported
22	30.5	2.5	1	4	22	5YR 4/6	yellowish red	spherical	sub-ang/-rnd	20	80		fine/med fine	well sorted	mature	uncnsld sedimemt	grain supported
23	33	1	1	4	23	5YR 4/6	yellowish red	spherical	sub-ang/-rnd	60	40		fine	well sorted	mature	uncnsld sedimemt	grain supported, bone
24	34	2	1	4	24	5YR 4/6	yellowish red	spherical	sub-angular	5	90	5	v fine/fine	well sorted	mature	uncnsld sedimemt	grain supported
25	36	1.5	1	4	25	5YR 5/6	yellowish red	sph/elong	sub-ang/-rnd	90	10		fine	well sorted	mature	uncnsld sedimemt	grain supported
26	37.5	3.5	1	5	26	5YR 4/6	yellowish red	spherical	sub-angular	15	85		fine	well sorted	mature	uncnsld sedimemt	grain supported
27 [b]	41	2	1	6	27	Hard Unit 6	red/brown/grey	poorly cnsld		10	70	20	fine/med ppt	well sorted	mature	Flowstone, CaCO3	prly cnsld, high fluid flow
28	43	2	1	7	28	5YR 5/6	yellowish red	spherical	sub-rounded	5	95		med fine	well sorted	mature	uncnsld sedimemt	grain supported
29	45	75/.25/.5	1	7	29	5YR 5/6	yellowish red	sph/elong	sub-ang/-rnd	95	5		fine	well sorted	mature	uncnsld sedimemt	grain supported, blackened bone
30	46	mix	1	7	mix 29/30	5YR 4/6	yellowish red	spherical	sub-angular	10	90		v fine/fine	well sorted	mature	uncnsld sedimemt	grain supported
31	46.5	5.5	1	7	30	5YR 4/6	yellowish red	spherical	sub-angular	10	90		fine	well sorted	mature	uncnsld sedimemt	grain supported
32 [a]	52	0.75	1	8	31	5YR 6/6	reddish yellow	spherical	sub-rounded	99	1		v fine	well sorted	mature	uncnsld sedimemt	grain supported
33	53.25	.75/.75	1	8	32	5YR 5/6	yellowish red	spherical	sub-rounded	40	60		fine	well sorted	mature	uncnsld sedimemt	grain supported
34	54.75	0.75	1	8	33	5YR 4/6	yellowish red	spherical	sub-rounded	40	60		fine	well sorted	mature	uncnsld sedimemt	grain supported
35	55.5	3	1	8	34	5YR 5/8	yellowish red	spherical	sub-rounded	40	60		fine/med fine	well sorted	mature	uncnsld sedimemt	grain supported
36	58.5	1.25	2	9	35	5YR 5/6	yellowish red	sph/elong	sub-ang/-rnd	90	10		fine	well sorted	mature	uncnsld sedimemt	grain supported
37	59.75	3.75	2	9	36	5YR 5/6	yellowish red	sph/elong	sub-ang/-rnd	90	10		fine	well sorted	mature	uncnsld sedimemt	grain supported
38	63.5	1	2	9	37	5YR 5/6	yellowish red	sph/elong	sub-ang/-rnd	90	10		fine	well sorted	mature	uncnsld sedimemt	grain supported
39	64.5	0.5	2	9	38	5YR 5/6	yellowish red	sph/elong	sub-ang/-rnd	95	5		v fine	well sorted	mature	uncnsld sedimemt	grain supported
40	65	0.5	2	9	39	5YR 4/6	yellowish red	spherical	sub-angular	1	99		v fine	well sorted	mature	uncnsld sedimemt	grain supported, clay bolus
-	unsampled zone	3	-	-	-	-	-	-	-				-	-	-	-	-
41	68	3	2	10	40	5YR 5/6	yellowish red	spherical	sub-ang/-rnd	98	2		fine/ing upward	well sorted	mature	uncnsld sedimemt	grain supported
42	71	4	2	11	41	5YR 4/6	yellowish red	spherical	sub-ang/-rnd	25	75		fine	well sorted	mature	uncnsld sedimemt	grain supported
43	75	0.5	2	11	42	5YR 4/6	yellowish red	spherical	sub-angular	5	95		fine	well sorted	mature	uncnsld sedimemt	grain supported
44 [a]	75.5	4.5	2	12	43	5YR 5/6	yellowish red	sph/elong	sub-ang/-rnd	98	2		v fine	well sorted	mature	uncnsld sedimemt	grain supported
45	80	1	2	12	44	5YR 6/6	reddish yellow	sph/elong	sub-ang/-rnd	99		1	v fine	well sorted	mature	uncnsld sedimemt	grain supported
46	81	5	2	12	45	5YR 5/8	yellowish red	spherical	sub-rounded	40	60		v fine	well sorted	mature	uncnsld sedimemt	grain supported
47	86	1.5	2	12	46	5YR 6/6	reddish yellow	sph/elong	sub-ang/-rnd	98	2		v fine	well sorted	mature	uncnsld sedimemt	grain supported
48	87.5	8.5	2	13	47	5YR 5/6	yellowish red	spherical	sub-ang/-rnd	60	40		v fine/fine	well sorted	mature	uncnsld sedimemt	grain supported
49	95	in above	2	13	48	5YR 5/6	yellowish red	spherical	sub-ang/-rnd	60	40		fine	well sorted	mature	uncnsld sedimemt	grain supported
50	96	1	2	13	49	5YR 5/6	yellowish red	spherical	sub-ang/-rnd	98	2		v fine	well sorted	mature	uncnsld sedimemt	grain supported
51	97	0.5	2	13	50	5YR 4/6	yellowish red	sph/elong	sub-ang/-rnd	40	60		v fine	well sorted	mature	uncnsld sedimemt	grain supported
52	97.5	1	2	13	51	5YR 5/4	reddish brown	sph/elong	sub-ang/-rnd	99	0	1	v v fine/silt	well sorted	mature	uncnsld sedimemt	grain supported
53	98.5	1.5	2	14	52	Hard	Chocolate brown	consolidated					fine/med ppt			Flowstone, calcite	matrix supported, bone fragments
	cnsld: consolidated			uncnsld: unconsolidated			[a] Level of dating samples					[b] Unit 6					

Table S6b. Area 3 and 4 sediments, individual grain descriptions for Specimen Cave.

number	profile Depth (cm)	thickness s (cm)	Area A	Unit U	Sample No (Small) S	Colour Code	Colour Name	Shape Sphericity	Shape Angularity	Composition QFL%			Texture	Sorting	Maturity	cementation	Description
55	0	5	3	floor	0	y limestone?	white/light grey	cnsold cave pieces					v fine			Limestone/Calcite	matrix supported
56	5	3	3	1	1	5YR 6/6	reddish yellow	spherical	sub-rounded	90	10		v fine/fine	well sorted	mature	uncnsld sedimemt	grain supported
57	8	3	3	1	2	Hard	green/grey/white	consolidated ppt					ppt			Flowstone, calcite	matrix supported
58	11	0.5	3	1	3	5YR 6/6	reddish yellow	spherical	sub-rounded	99	1		v fine/fine	well sorted	mature	uncnsld sedimemt	grain supported
59	11.5	1	3	1	4	Hard	green/grey/white	consolidated ppt				5	ppt			Flowstone, calcite	matrix supported
60	12.5	0.5	3	1	5	5YR 6/6	reddish yellow	sph/elong	sub-angular	95	5		fine	well sorted	mature	uncnsld sedimemt	grain supported
61	13	1	3	1	6	Hard	choc brown/olive green	consolidated ppt					v fine ppt			Flowstone, calcite	matrix supported
62	14	2	3	1	7	5YR 5/6	yellowish red	sph/elong	sub-ang/-rnd	80	10	10	medium	well sorted	mature	uncnsld sedimemt	grain supported
63	16	3	3	1	8	Hard	tan/beige	consolidated ppt					ppt			Flowstone, calcite	matrix supported
64	19	6	3	2	9	5YR 6/6	reddish yellow	spherical	sub-angular	90	5	5	fine/medium	well sorted	mature	uncnsld sedimemt	grain supported
65	25	1	3	2	10	5YR 4/4	reddish brown	semi-cnsld brittle					med	well sorted	mature	uncnsld sedimemt	grain supported
66	26	1	3	2	11	5YR 5/8	yellowish red	spherical	sub-rounded	98	2		fine	well sorted	mature	uncnsld sedimemt	grain supported
67	27	2	3	3	12	Hard	white	consolidated					ppt			Flowstone, calcite	matrix supported
68	29	1	3	3	13	Hard	dark choc brown/grey	consolidated					ppt			Flowstone, calcite	matrix supported
69	30	3	3	3	14	5YR 4/6	yellowish red	spherical	sub-rounded	10	80	10	medium	well sorted	mature	uncnsld sedimemt	grain supported
70	33	3	3	3	15	Hard	choc brown/grey	consolidated					ppt	well sorted	mature	uncnsld sedimemt	grain supported
71	38	16	3	4	16	5YR 4/6	yellowish red	spherical	sub-rounded	60	40		fine	well sorted	mature	uncnsld sedimemt	grain supported
72 [a]	45	in above	3	4	17	5YR 4/6	yellowish red	spherical	sub-rounded	60	40		fine	well sorted	mature	uncnsld sedimemt	grain supported
73	51	in above	3	4	18	YR 4/6 (5/6)	yellowish red	spherical	sub-rounded	60	40		fine	well sorted	mature	uncnsld sedimemt	grain supported
	52.5 slope to 56																
74	52.5	3.5	lope 3-4	5	93	5YR 4/6	yellowish red	spherical	sub-rounded	10	90		fine	well sorted	mature	uncnsld sedimemt	grain supported
75	56	2	4	5	94	Hard	green/grey/brown	cnsld ppt fine banded layers					fine ppt banded			Flowstone, calcite	matrix supported
76	58	25/.75/.5	4	5	95	'R 4/6 - Hard	yellowish red - brown/re(	cnsld layers & v fine clay layers					fine ppt	well sorted	mature	uncnsld sedimemt	grain supported/matrix
77	60	.25/.5/.5	3-4	5	96	'R 4/6 - Hard	yellowish red - brown/re(	cnsld layers & v fine clay layers					fine ppt	well sorted	mature	uncnsld sedimemt	grain supported/matrix
78	62	1	3-4	5	97	5YR 4/6	yellowish red	spherical	sub-rnd/rnd	60	40		fine/medium	well sorted	mature	uncnsld sedimemt	grain supported
79	63	1.5	3-4	5	98	Hard	brown/red/green - grey/\	cnsld ppt fine banded layers					fine ppt			Flowstone, calcite	matrix supported
80	64.5	0.5	3-4	5	99	5YR 4/6	yellowish red	spherical	sub-rounded	40	60		fine/medium	well sorted	mature	uncnsld sedimemt	grain supported
81 [b]	65	2	3-4	6	100	Hard	grey/white	cnsld ppt					fine ppt			Flowstone, calcite	matrix supported
82	65	in above	4	6	100z	Hard		cnsld ppt, holey, behive shape					fine ppt			Flowstone, bone?	matrix supported
83	65	in above	4	6	100y	Hard		cnsld ppt, bone fragments					fine ppt			Flowstone, bone?	matrix supported
84	67	1.5	4	7	101	5YR 5/6	yellowish red	spherical	sub-rnd/rnd	90	10		medium	well sorted	mature	uncnsld sedimemt	grain supported
85	68.5	6	4	7	102	5YR 4/6	yellowish red	spherical	sub-angular	10	80	10	fine	well sorted	mature	uncnsld sedimemt	grain supported
86	74.5	1/.5/1	4	7	103	5YR 4/6	yellowish red	spherical	sub-angular	80	20		fine/medium	well sorted	mature	uncnsld sedimemt	grain supported
87	77	16	4	8	104	5YR 4/6	yellowish red	spherical	sub-angular	5	95		fine/medium	well sorted	mature	uncnsld sedimemt	grain supported
88	82.5	in above	4	8	105	5YR 4/6	yellowish red	spherical	sub-angular	5	95		fine/medium	well sorted	mature	uncnsld sedimemt	grain supported
89 [a]	88	in above	4	8	106	5YR 4/6	yellowish red	spherical	sub-angular	5	95		fine/medium	well sorted	mature	uncnsld sedimemt	grain supported
90	93	2	4	9	107	5YR 6/6	reddish yellow	sph/elong	sub-ang/-rnd	99	1		v fine	well sorted	mature	uncnsld sedimemt	grain supported
	95	??	Hard layer at base - either calcite/flowstone or bone or mix														

cnsld: consolidated   uncnsld: unconsolidated   [a] Level of dating samples   [b] Unit 6

Table S7. Grain size analysis particle fractions percentage of each sieved size of the twelve samples using the Wentworth-Uden scale.

Wentworth size class	Fine silt & clay	Coarse silt	Very fine sand	Fine Sand	Medium sand	Coarse sand*	
Opening (mm)	Pan	0.038	0.063	0.125	0.25	0.5	
Phi (φ)	>4.71	4.71	4.00	3.00	2.00	1.00	
Sample	%	%	%	%	%	%	Total %
Z25	0.22	0.78	2.89	27.67	53.11	15.33	100.00
Z23	1.00	1.71	3.00	27.00	42.57	24.71	100.00
Z21	0.88	1.50	4.50	28.63	36.00	28.50	100.00
Z19	1.33	1.78	3.89	24.22	34.67	34.11	100.00
Z17	1.33	2.33	4.44	20.33	21.89	49.67	100.00
Z15	0.20	0.60	2.50	38.70	49.00	9.00	100.00
Z13	0.70	0.70	2.10	29.90	52.30	14.30	100.00
Z11	0.25	0.88	1.88	31.38	53.13	12.50	100.00
Z9	0.70	0.70	3.10	24.90	34.30	36.30	100.00
Z6	0.25	0.25	2.00	28.88	54.25	14.38	100.00
Z3	0.70	0.70	2.00	26.10	46.40	24.10	100.00
Z1	1.60	2.00	4.50	26.00	28.50	37.40	100.00

*including cave pieces and fossil fragments

Geochemistry

Twelve of the large samples (Table 2) collected were weighed out to 10 g air dried lots, homogenised (Retsch PM100 ball mill) and 10 g wet lots for each sample and sent for XRF and XRD analysis at University of Wollongong, NSW. The 3 U-channel sections were wrapped in plastic in situ, and kept refrigerated until sent for surface XRF (Itrax) scanning at ANSTO, Lucas Heights, NSW. Further analysis of all of the raw scan data was completed in Microsoft Excel© and edited in CorelDRAW© 2018.

Itrax Sections are stored at PELL at the University of Adelaide. Further analysis of raw Itrax data was performed in Microsoft Excel© spreadsheets (Fig. S5 and S5).

Palynology

Four locations were tested for pollen content, of the ten samples collected only four were tested based on a shortened process of analysis (Nguyen, c2013) and found to be negative. The shortened process and reduce number of samples tested was based on information from another cave in the area being negative for pollen content. Samples were wet sieved, chemically separated and the upper (floating) layer syphoned off, the recovered fraction was added to a slide with coverslip and examined under 400x and 600x microscope.

Itrax
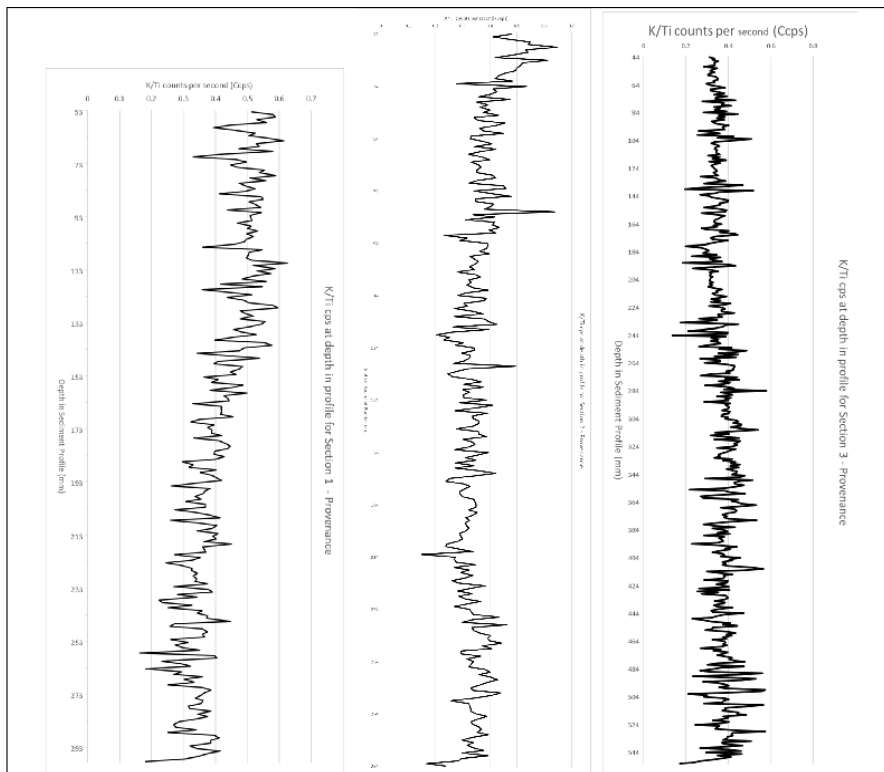
Figure S5. Section 1, 2 and 3: potassium/titanium (K/Ti) ratio for sediment provenance and climate indications.
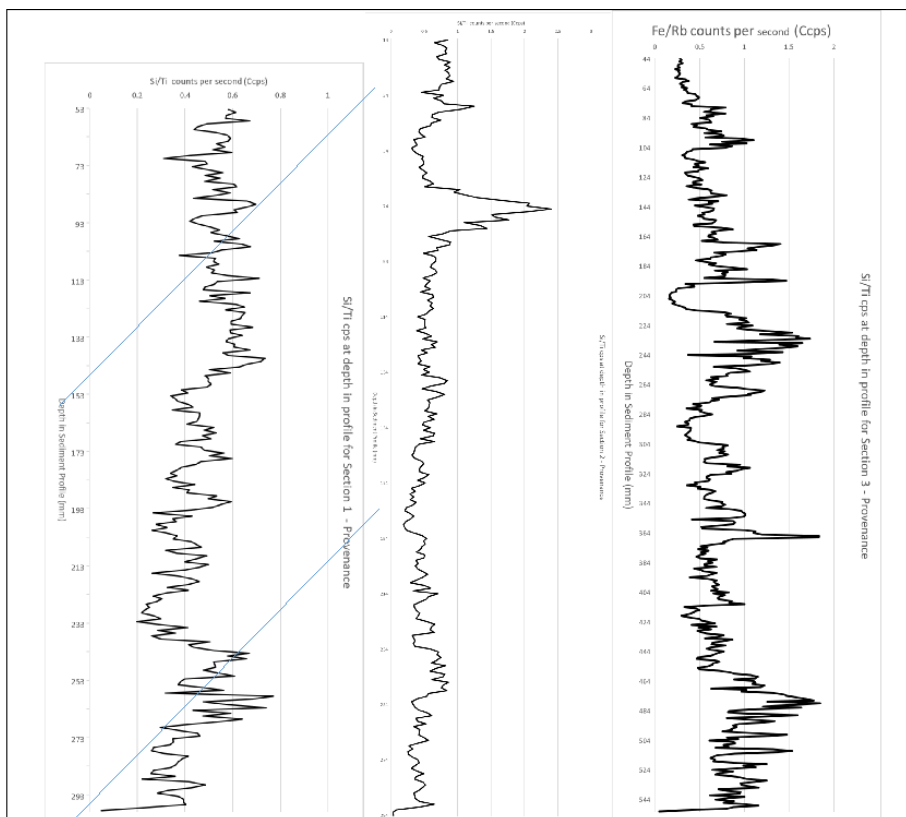
Figure S6. Section 1, 2 and 3: Si/Ti for aeolian input (increase to right means, increased sediment input – aeolian; increase to left means decreased sediment input).

Table S8. Pollen assay Specimen Cave, unconsolidated sediment samples by smear slide examined for pollen under 600x microscope. All 10 ml samples initially sieved to <250 μm fraction then further sieved to <100 μm fraction (**Date: Prepared** 29/05/18; **Analysed** 6/06/18)

Pollen (P)	Location (A/U/S)*	Results
P1	A1/U1/S01	No pollen present
P5	A2/U11/S42	No pollen present
P8	A3/U4/S17	No pollen present
P10	A4/U8/S106	No pollen present

*Area/Unit/Sample

SI References

AITKEN, M.J. (1998). An Introduction to Optical Dating: The Dating of Quaternary Sediments by the Use of Photon-Stimulated Luminescence. Oxford University Press, Oxford, 267 p.

ARNOLD, L. J., DEMURO, M., SPOONER, N. A., PRIDEAUX, G. J., MCDOWELL, M. C., CAMENS, A. B., . . . CARBONELL, E. (2018). Single-grain TT-OSL bleaching characteristics: Insights from modern analogues and OSL dating comparisons. *Quaternary Geochronology*. doi:10.1016/j.quageo.2018.01.004.

NGUYEN, N., et. al. (c2013). Palynology and Geochemistry Data And Methods, and Section Age Model: Supplementary Information.

PRESCOTT, J.R., HUTTON, J.T. (1994). Cosmic ray contributions to dose rates for luminescence and ESR dating: large depths and long-term time variations. *Radiation Measurements* (230, 497-500.

KELTS, K. (1998). Components In lake sediments: smear slide identifications, LRC Core Facility, The University of Minnesota.

LINNENLUCKE, L. P. (2012). *Single-grain optically stimulated luminescence (OSL) dating of terminal Pleistocene and early Holocene human occupation sites in the Dhofar region of Oman.* (Bachelor of Science (Honours), School of Earth & Environmental Science, Honours), University of Wollongong, Retrieved from http://ro.uow.edu.au/thsci/61.

MURRAY, A. S., & WINTLE, A. G. (2000). Luminescence dating of quartz using an improved single aliquot regenerative-dose protocol. *Radiation Measurements*(32), 57-73.

WANG, X. L., WINTLE, A. G., & LU, Y. C. (2006). Thermally transferred luminescence in fine-grained quartz from Chinese loess: Basic observations. *Radiation Measurements*(41), 649-658. doi:10.1016/j.radmeas.2006.01.001.

WOOKEY, ATKINSON, A., & DAY, A. (1995). Expedition Surveying Guide, Cambridge University Caving Club, [accessed March 2018] <https://www.sat.dundee.ac.uk/~arb/speleo/gpfseminar96/survey.html>.